

23

ABSTRACT

24 The dynamic and thermodynamic mechanisms that link retreating sea ice to increased
25 Arctic cloud amount and cloud water content are unclear. Using the fifth generation of the
26 ECMWF Reanalysis (ERA5), the long-term changes between years 1950-1979 and 1990-2019 in
27 Arctic clouds are estimated along with their relationship to sea-ice loss. A comparison of ERA5 to
28 CERES satellite cloud fractions reveals that ERA5 simulates the seasonal cycle, variations, and
29 changes of cloud fraction well over water surfaces during 2001-2020. This suggests that ERA5
30 may reliably represent the cloud response to sea-ice loss because melting sea ice exposes more
31 water surfaces in the Arctic. Increases in ERA5 Arctic cloud fraction and water content are largest
32 during October-March from ~950-700 hPa over areas with significant ($\geq 15\%$) sea-ice loss. Further,
33 regions with significant sea-ice loss experience higher convective available potential energy (~2-
34 2.75 J kg^{-1}), planetary boundary layer height (~120-200 m) and near-surface specific humidity
35 (~0.25-0.40 g kg^{-1}) and a greater reduction of the lower tropospheric temperature inversion (~3-4
36 $^{\circ}\text{C}$) than regions with small (<15%) sea-ice loss in autumn and winter. Areas with significant sea-
37 ice loss also show strengthened upward motion between 1000-700 hPa, enhanced horizontal
38 convergence (divergence) of air, and decreased (increased) relative humidity from 1000-950 hPa
39 (950-700 hPa) during the cold season. Analyses of moisture divergence, evaporation minus
40 precipitation, and meridional moisture flux fields suggest that increased local surface water fluxes,
41 rather than atmospheric motions, provide a key source of moisture for increased Arctic clouds over
42 newly exposed water surfaces from October-March.

43

SIGNIFICANCE STATEMENT

44 Sea-ice loss has been shown to be a primary contributor to Arctic warming. Despite the
45 evidence linking large sea-ice retreat to Arctic warming, some studies have suggested that
46 enhanced downwelling longwave radiation associated with increased clouds and water vapor is
47 the primary reason for Arctic amplification. However, it is unclear how sea-ice loss is linked to
48 changes in clouds and water vapor in the Arctic. Here, we investigate the relationship between
49 Arctic sea-ice loss and changes in clouds using the ERA5 reanalysis dataset. Improved knowledge
50 of the relationship between Arctic sea-ice loss and changes in clouds will help further our
51 understanding of the role of the cloud feedback in Arctic warming.

52 **1. Introduction**

53 Arctic sea ice has been declining over recent decades, accompanied by a lengthening melt
54 season (Stroeve et al. 2014). Loss of sea-ice concentration (SIC) enhances oceanic absorption of
55 solar radiation in summer and oceanic release of upward longwave (LW) radiation, sensible (SH)
56 and latent (LH) heat fluxes during the cold season due to a steep temperature gradient between the
57 warm ocean surface and frigid overlying air (Royer et al. 1990; Deser et al. 2010; Boeke and
58 Taylor 2018). Increased oceanic heating due to sea-ice loss has been shown to drive Arctic
59 amplification (AA) – the enhanced surface and lower tropospheric warming in the Arctic relative
60 to the rest of the world under increasing greenhouse gases (GHGs) (Screen and Simmonds 2010a,
61 2010b; Serreze and Barry 2011; Boeke and Taylor 2018; Dai et al. 2019). Further, exposed ocean
62 water surfaces are associated with greater cloud fraction and cloud water content than ice-covered
63 surfaces during Arctic autumn (e.g., Kay and Gettelman 2009; Eastman and Warren 2010; Liu et
64 al. 2012; Taylor et al. 2015; Kay et al. 2016; Morrison et al. 2018, 2019). As the Arctic continues
65 to warm and lose sea ice under rising GHGs, Arctic cloud amount is projected to increase during
66 the cold season (Vavrus et al. 2009; Philipp et al. 2020). Cloud radiative feedbacks account for a
67 portion of Arctic warming under increased GHGs by enhancing surface downwelling LW radiation
68 (Vavrus 2004; Taylor et al. 2013); however, clouds also cool the Arctic in summer by reflecting
69 shortwave (SW) radiation back to space (Curry et al. 1996; Intrieri et al. 2002b; Jenkins and Dai
70 2021). Changes in Arctic cloud radiative forcing (CRF) impact not only surface temperature but
71 also sea-ice extent (Choi et al. 2014; Burt et al. 2016). The complex effects of clouds on Arctic
72 energy budget and surface warming motivate further investigation into the local cloud response to
73 observed sea-ice loss.

74 Clouds play an important role in Arctic top-of-the-atmosphere (TOA) and surface energy
75 balances (Wetherald and Manabe 1988; Intrieri et al. 2002b; Shupe and Intrieri 2004). Jenkins and
76 Dai (2022) showed that clouds contributed $\sim 3 \text{ W m}^{-2}$ ($-0.25 \sim -2 \text{ W m}^{-2}$) of TOA forcing during
77 October-March (May-July) from 1950-1979 to 1990-2019 based on analyses of the fifth generation
78 of the European Center for Medium Range Weather Forecasts reanalysis (ERA5). Further, they
79 found that the spatial patterns of Arctic cloud feedback are strongly correlated with sea-ice changes
80 in autumn and winter but not in summer. Monroe et al. (2021) found a strong cloud response to
81 wintertime polynyas (i.e., a region with anomalously low SIC). During polynya events, cloud

82 fractions and water contents are larger over the polynya than over surrounding ice-covered regions.
83 Increases in surface downward LW radiation due to enhanced cloudiness over the open water slows
84 refreezing of the sea ice, lengthening polynya events (Monroe et al. 2021). The SW cooling effects
85 of clouds also influence Arctic sea-ice extent. Choi et al. (2014) suggest that years with strong
86 cloud cooling and thus reduced surface absorption of solar radiation in spring and early summer
87 increases late summer Arctic sea-ice extent. Other studies confirm that springtime cloud warming
88 in spring is associated with low September sea-ice anomalies (Kapsch et al. 2013; Cox et al. 2016;
89 Huang et al. 2019). Further, summer CRF becomes more negative under conditions with low SIC
90 due to the high contrast in albedo between clouds and the underlying ocean surface (Alkama et al.
91 2020).

92 Previous studies have shown a strong (weak) Arctic cloud response to sea-ice variations
93 and changes during autumn (summer) using observations (Kay and Gettelman 2009; Palm et al.
94 2010; Taylor et al. 2015; Morrison et al. 2018), reanalysis products (Schweiger et al. 2008;
95 Cuzzone and Vavrus 2011), and model simulations (Vavrus et al. 2011; Barton and Veron 2012;
96 Morrison et al. 2019). Kay and Gettelman (2009) analyzed the cloud-sea ice relationship during
97 2006-2008 using satellite observations and found that Arctic low cloud fraction was higher over
98 open water surfaces than ice-covered surfaces in September, but not in summer (i.e., June-July-
99 August). During the warm summer months, Arctic total cloud fraction depended more on synoptic
100 variability rather than the type of the underlying surface (i.e., ice-covered or open water), while
101 clouds in autumn depended on both the surface types and background atmospheric circulation
102 (Kay and Gettelman 2009). Palm et al. (2010) also found an enhancement of clouds between 0.5-
103 2 km over open water surfaces relative to ice-covered surfaces in early autumn using satellite data
104 during 2003-2007. These studies attributed the increased cloud cover to enhanced surface energy
105 and moisture fluxes, a deeper planetary boundary layer, and decreased lower tropospheric stability
106 over exposed ocean waters. A recent modeling study confirmed that exposed water surfaces
107 enhance low cloud formation in winter (Zheng and Ming 2023).

108 Schweiger et al. (2008) found a decrease in Arctic low clouds below 800 hPa, but an
109 increase in Arctic mid-level clouds between 800-450 hPa during years with anomalously low SIC
110 during 1980-2001 in ERA-40 reanalysis data. This finding differs from other studies that reported
111 larger increases in low clouds than mid-level clouds over exposed ocean surfaces (Kay and

112 Gettelman 2009; Palm et al. 2010; Morrison et al. 2018, 2019). Schweiger et al. (2008) suggest
113 that large near-surface warming associated with low SIC reduces the static stability of the lower
114 troposphere, enhancing vertical mixing and thus mid-level cloud cover. Further, they found that
115 under low SIC conditions, the relative humidity (RH) from 1000-950 hPa decreased, diminishing
116 cloud cover near the surface. Model simulations confirm decreased RH between 1000-950 hPa,
117 but increased RH above 950 hPa, leading to suppressed (enhanced) cloud fraction below (above)
118 950 hPa (Abe et al. 2016) in response to Arctic sea-ice loss. Thus, there still exist inconsistencies
119 regarding how low and middle clouds may respond to sea-ice loss. An improved understanding of
120 the vertical profiles of cloud properties, and the dynamic and thermodynamic processes
121 influencing Arctic cloud profiles is needed because cloud height influences CRF and cloud
122 feedback (Zelinka et al. 2012).

123 The primary goals of this study are to analyze the seasonality, vertical structure, and spatial
124 patterns of Arctic cloud property changes (i.e., in cloud fraction, and cloud liquid and ice water
125 contents) over areas with and without significant sea-ice loss from ERA5 data and to improve
126 understanding of the atmospheric conditions that link sea-ice loss to enhanced cloud amount.
127 Specifically, we seek to answer the following questions:

- 128 1. How is the long-term sea-ice loss from 1950-2019 related to changes in Arctic clouds at
129 different levels, atmospheric stability, and other related fields in terms of their spatial
130 patterns, seasonality, and physical linkages?
- 131 2. What dynamic and thermodynamic processes drive increases in Arctic cloud fraction
132 and/or cloud water content in response to sea-ice loss and how do changes in these dynamic
133 and thermodynamic processes vary seasonally?
- 134 3. Do increases in Arctic cloud properties over areas with sea-ice loss result from enhanced
135 remote moisture transport or increased local evaporation due to sea-ice loss?

136 A better understanding of the local cloud response to Arctic sea-ice loss will improve estimates of
137 Arctic cloud feedback, which is a major source of uncertainty in future climate projections (Soden
138 et al. 2004; Gettelman and Sherwood 2016; Ceppi et al. 2017).

139 In this study, we make use of the ERA5 reanalysis dataset (Hersbach et al. 2020) to
140 investigate changes in Arctic cloud properties and atmospheric conditions over areas with and

141 without significant sea-ice loss between 1950-1979 and 1990-2019. Our focus on long-term
142 changes distinguishes our study from early work that analyzed the cloud response to sea-ice
143 variations and changes over shorter time periods (e.g., Schweiger et al. 2008; Kay and Gettelman
144 2009; Morrison et al. 2018). After introducing the data and methods in Section 2, we evaluate
145 ERA5 cloud fraction against satellite-based products in Section 3. We then document the spatial
146 patterns, vertical profiles, and seasonality of long-term Arctic cloud changes in ERA5 in Section
147 4 and describe the changes in atmospheric conditions over areas with significant sea-ice loss and
148 explore their physical linkages to Arctic cloud changes in Section 5. We summarize and discuss
149 the results in Section 6. Our findings suggest new mechanisms and synthesize previous findings
150 that may link sea-ice loss to Arctic cloud changes.

151 **2. Data and Methods**

152 *a. ERA5 Reanalysis*

153 As long-term observations over the Arctic Ocean are sparse, we use monthly data from
154 1950-2019 from ERA5 reanalysis (Hersbach et al. 2020) on a 1.0° latitude/longitude grid. We
155 analyze three-dimensional fields of cloud fraction, and specific cloud liquid and ice water contents.
156 Further, we examine changes in SIC, surface air temperature, convective available potential energy
157 (CAPE), planetary boundary layer height (PBLH), vertically integrated moisture divergence, total
158 precipitation, surface evaporation, and vertical profiles of air temperature, vertical velocity,
159 horizontal divergence, specific humidity, and relative humidity. We select the 1000, 950, 900, 850,
160 700, 600, and 500 hPa levels for three-dimensional variables. Graham et al. (2019b) showed that
161 ERA5 outperforms other reanalysis datasets in reproducing vertical profiles of temperature, wind,
162 and specific humidity in the Arctic region. ERA5 SIC incorporates the second version of the
163 Hadley Centre Global Sea Ice and Sea Surface Temperature (HadISSTv2) product for years 1950-
164 1978 and the Operational Sea Surface Temperature and Ice Analysis (OSTIA) for 1979 to the
165 present (Hersbach et al. 2020). We use ERA5 SIC fields because satellite-based sea ice
166 observations are not available prior to 1979. Both OSTIA and HadISSTv2 produce similar
167 interannual variability and trends for Arctic SIC, especially over areas that are predominantly ice-
168 covered (i.e., $SIC \geq 50\%$). For areas where $SIC \geq 10\%$, OSTIA Arctic-mean SIC is slightly greater
169 than HadISSTv2 for 1979-2019. We do not expect any discrepancies in ERA5 SIC to affect our

170 conclusions because ERA5 captures the interannual variability, seasonal cycle, and trends in Arctic
171 sea-ice well for the post-satellite period (Hirahara et al. 2016).

172 We focus on the changes in cloud properties and atmospheric conditions between years
173 1950-1979 and 1990-2019. Local air temperatures remained stable during 1950-1979, but large
174 Arctic warming occurred from 1990-2019 (England et al. 2021). Thus, the 1990-2019 minus 1950-
175 1979 difference estimates how recent sea-ice loss may have impacted Arctic cloud properties and
176 atmospheric conditions, even though ocean-atmosphere interactions are two-way. ERA5
177 incorporates observations of surface pressure, temperature, and wind speed from a variety of
178 historical archives (e.g., the International Surface Pressure Databank, the Comprehensive
179 Historical Upper Air Network, etc) to generate data prior to 1979. Confidence in the ERA5 data
180 increases from 1950 to 1978, where the number of observations incorporated into the reanalysis
181 increases from ~53,000 to 570,000 observations per day (Bell et al. 2021). The 1980-1989 decade
182 experienced small local warming in the Arctic region relative to years 1990-2019 and is excluded
183 from the analysis. However, a linear trend analysis for years 1980-2020 reveals similar spatial
184 patterns of cloud changes as the long-term difference (not shown). Therefore, we do not expect
185 exclusion of years 1980-1989 to qualitatively affect our conclusions.

186 To assess the impact of sea-ice loss on Arctic clouds and atmospheric conditions, we
187 separate the Arctic Ocean into areas with significant ($\geq 15\%$) or little ($< 15\%$) SIC loss (excluding
188 land) between 1950-1979 and 1990-2019. Areas with 15% or greater sea-ice loss are located
189 mostly along the 1950-1979 marginal ice zones, which became mostly open water by 1990-2019.
190 We average and group the data by month for each 30-year period to examine the mean seasonal
191 cycle and its change for each variable. Huang et al. (2019) showed that the atmosphere and ocean
192 are tightly coupled in March, but the influence of sea ice on the atmosphere weakened from April-
193 June. Thus, we define the cold (warm) season as October-March (April-September) to investigate
194 the role of strong (weak) ocean-atmosphere coupling on cloud-sea ice interactions. The Arctic
195 region is mainly ocean surface north of the Arctic Circle; therefore, we define the Arctic as the
196 region poleward of 67°N for area-weighted averages. However, we show the region poleward of
197 55°N to include the Sea of Okhotsk and Hudson Bay on maps. We estimate the statistical
198 significance of temporal and spatial correlations with a two-tailed Student t -test. For this study, a
199 statistically significant correlation has an associated p -value less than 0.01.

200 ERA5 cloud properties are based on the Tiedtke (1993) cloud scheme, which estimates
201 clouds by resolving processes that are cloud water sources (e.g., condensation, sublimation, or
202 cumulus convection) or sinks (e.g., precipitation or cloud evaporation). Yeo et al. (2022) evaluated
203 Arctic clouds in ERA5 by comparing ERA5 cloud properties to CloudSat and Cloud-Aerosol Lidar
204 and Infrared Pathfinder Satellite Observation (CloudSat-CALIPSO) data for July 2006 to June
205 2010. For cloud fraction, ERA5 simulates too many clouds over sea ice relative to ocean water
206 surfaces. Further, ERA5 underestimates cloud liquid and ice water path relative to satellite
207 observations over the entire Arctic region. Despite these mean biases, ERA5 produces a reasonable
208 seasonal cycle of Arctic mid-level (i.e., 800-450 hPa) cloud fraction, high (i.e., ≤ 450 hPa) cloud
209 fraction, liquid water path, and ice water path, suggesting that ERA5 captures the seasonality of
210 Arctic clouds properties well. Further, the discrepancy between CloudSat-CALIPSO and ERA5
211 mean low cloud fraction and cloud vertical profiles are reduced over open water surfaces compared
212 to ice-covered areas (Yeo et al. 2022). Due to the potential biases in ERA5 cloud variables, we
213 compare ERA5 cloud fraction and CRF to data from the Clouds and the Earth's Radiant Energy
214 System (CERES; Wielicki et al. 1996) project.

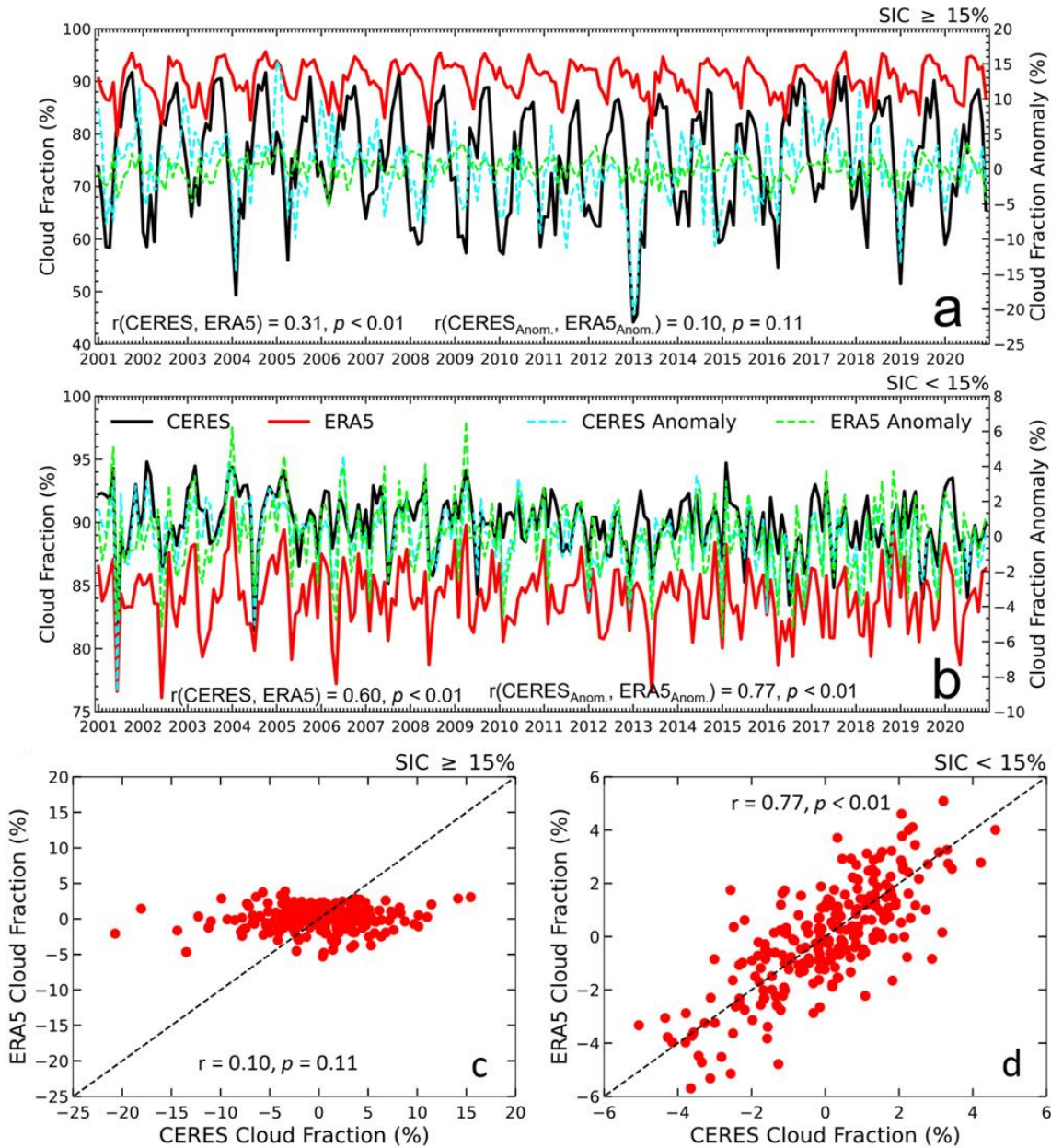
215 *b. CERES Energy Balanced and Filled Data*

216 We compare monthly ERA5 cloud fraction and CRF data to those from version 4.1 of the
217 CERES (specifically its energy balanced and filled dataset - EBAF; Loeb et al. 2018) from January
218 2001 to December 2020. Cloud fraction in CERES is based on observations from the Moderate
219 Resolution Imaging Spectroradiometer (MODIS) for both daytime and nighttime. MODIS uses
220 passive remote sensing techniques that rely on reflected SW radiation and emitted LW radiation
221 to infer radiative fluxes and cloud properties. In the Arctic region, MODIS underestimates clouds
222 over sea ice (by ~10-20%) especially at night due to the low contrast in albedo and thermal
223 emissions between clouds and ice-covered surfaces (Liu et al. 2010). CloudSat-CALIPSO satellite
224 observations (that rely on active remote sensing) are also commonly used to study Arctic cloud
225 properties (e.g., Taylor et al. 2015; Morrison et al. 2018), but data poleward of 82°N are unreliable
226 due to an insufficient number of observations (e.g., Liu et al. 2010; Taylor et al. 2015). Further,
227 CloudSat-CALIPSO may not capture clouds below 1 km well due to surface clutter and/or
228 attenuation of the lidar beam used to retrieve atmospheric conditions (Intrieri et al. 2002a;
229 Zygmuntowska et al. 2012).

230 We compare total cloud fraction and CRF from CERES and ERA5 over their period of
231 overlap (i.e., 2001-2020). Combined observations from the *Terra* and *Aqua* satellites are included
232 after July 2002 in CERES, but data only from *Terra* are available prior to this date. To roughly
233 estimate the impact of SIC on cloud fractions and other related fields in ERA5 and CERES, we
234 compute averages over areas where the mean SIC for 2001-2020 is less than 15% (excluding land)
235 and over regions where the mean SIC is 15% or more. We also compare the seasonal cycle of the
236 CRF at both the TOA and surface from ERA5 and CERES, where the CRF is defined as the all-
237 sky minus clear-sky total (i.e., SW+LW) radiative flux difference. Note that MODIS does not
238 directly measure cloud liquid and ice water contents. We emphasize that section 3 includes only a
239 brief comparison of ERA5 cloud fraction to one satellite-based product, and that other studies (e.g.,
240 Yeo et al. 2022) provide a more detailed evaluation of Arctic clouds in reanalysis datasets.

241 **3. Comparison of CERES and ERA5 Cloud Fraction and CRF**

242 The timeseries of Arctic-mean monthly cloud fraction from ERA5 and CERES are closely
243 related when averaged over ocean water surfaces ($r = 0.60$, $p < 0.01$; Fig. 1b), but are less well
244 correlated when averaged over areas containing sea ice ($r = 0.31$, $p < 0.01$; Fig. 1a). After removing
245 the mean seasonal cycle, which is largest in CERES over sea ice, the correlations change to 0.77
246 (Fig. 1b, d) and 0.10 (Fig. 1a, c) over Arctic water and ice surfaces, respectively. Cloud fraction
247 over sea ice-covered surfaces tend to be higher in ERA5 (~85-95%) than CERES (~50-90%),
248 partly due to the underestimation of cloud fraction over sea ice by MODIS (Liu et al. 2010);
249 however, the seasonal variations are much smaller in ERA5 than CERES over sea ice (Fig. 1a).
250 Over water surfaces, the ERA5 and CERES cloud fractions show comparable amplitudes of
251 variations, with CERES exhibiting slightly greater cloud amount (i.e., ~87% for ERA5 versus
252 ~92% for CERES) (Fig. 1b).

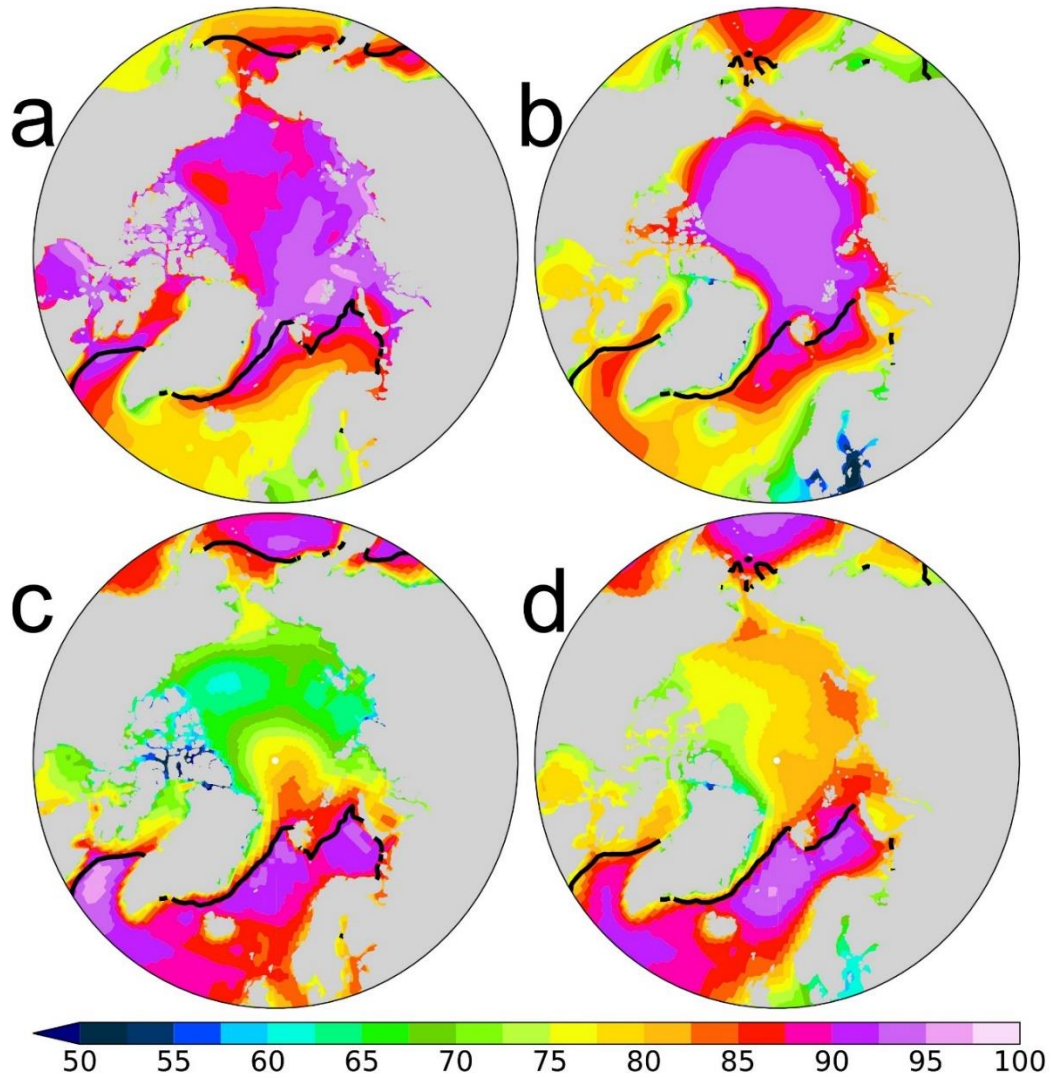


253

254 **Fig. 1.** (a, b) Timeseries of monthly cloud fraction (in %) from January 2001 to December 2020
 255 averaged over oceanic areas with 2001-2020 annual mean sea-ice concentration (a) greater than
 256 or equal to 15% or (b) less than 15% for ERA5 (solid red and dashed green lines) and CERES
 257 (solid black and dashed cyan lines) data with the seasonal cycle included (left y-axis; solid lines)
 258 and mean seasonal cycle removed (right y-axis; dashed lines). The correlation coefficient (r) and
 259 associated p -value between the timeseries is shown. (c, d) ERA5 vs. CERES monthly Arctic (67°-
 260 90°N) cloud fraction (in %; years 2001-2020; mean seasonal cycle removed) averaged over ocean
 261 surfaces for areas with (c) mean SIC $\geq 15\%$ or (d) mean SIC $< 15\%$.
 262

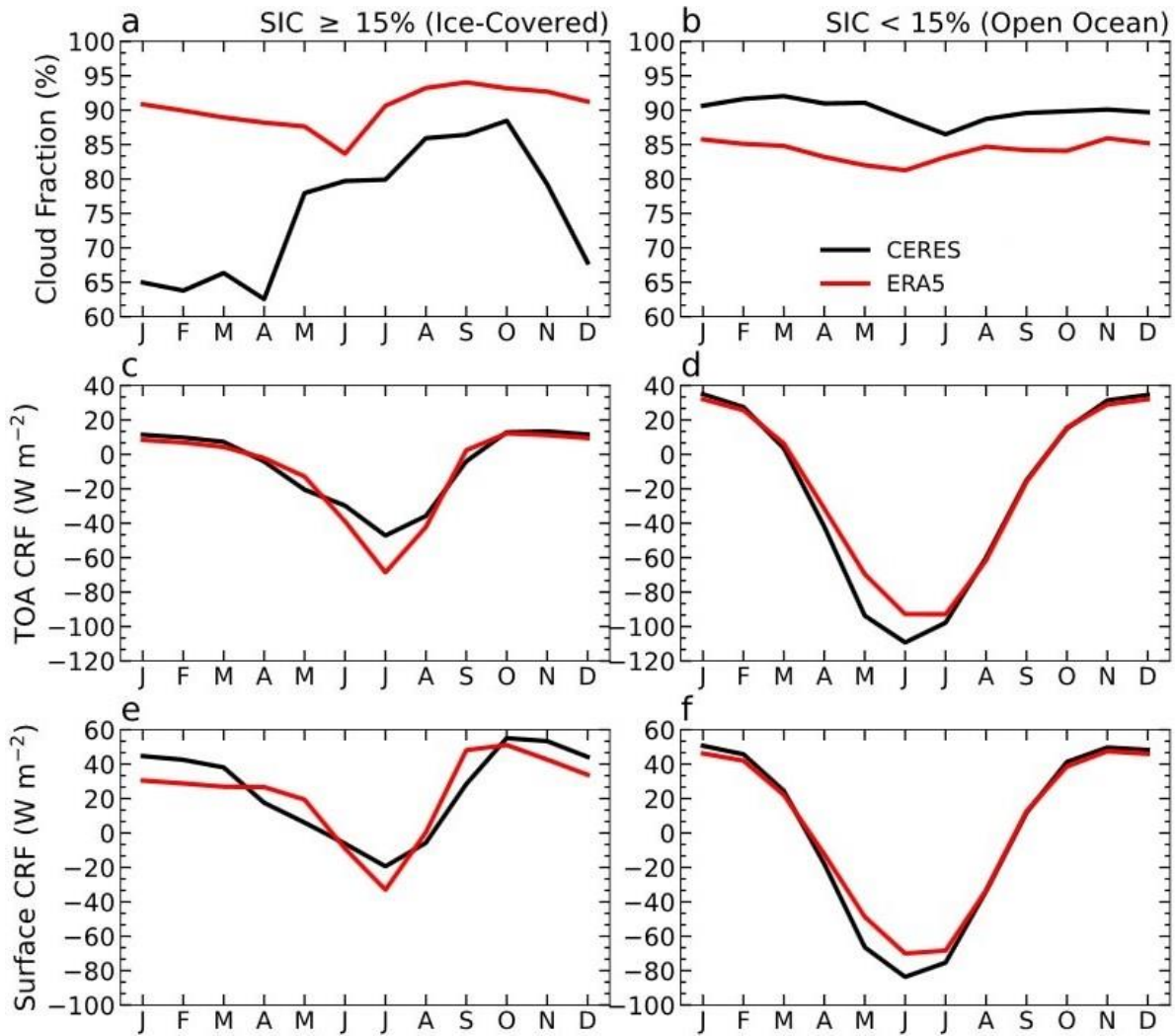
263 Next, we examine the spatial patterns (Fig. 2) and seasonal cycles (Fig. 3a-b) of the 2001-
 264 2020 mean Arctic cloud fraction in ERA5 and CERES. Spatially, ERA5 mean cloud amounts are

265 ~90-100% over areas poleward of the 15% mean sea ice edge in each season, higher than open-
266 water ocean surfaces (Fig. 2a-b). In contrast, cloud fraction in CERES are generally lower over
267 sea-ice covered areas than open-water ocean surfaces (Fig. 2c-d), especially from October-March
268 (Fig. 2c). The MODIS clouds used in CERES likely overestimate the water-versus-ice difference
269 due to its underestimation of clouds over sea ice (Liu et al. 2010). High lower-tropospheric stability
270 over ice-covered surfaces contributes to enhanced cloud cover over sea ice relative to open-water
271 ocean surfaces in ERA5 (Yeo et al. 2022). The discrepancy of total cloud fraction over sea ice is
272 also present in the seasonal cycle of cloud fraction, with the ERA5 showing a weak minimum in
273 June while the CERES shows elevated cloudiness from May-October (Fig. 3a), partly due to its
274 underestimation of cloudiness over sea ice during the polar night in the winter months (Liu et al.
275 2010). Cloud fraction averaged over open-water ocean surfaces does not vary significantly
276 throughout the year in both CERES and ERA5, with slightly higher cloud fraction in CERES (Fig.
277 3b). The difficulties in measuring clouds over Arctic sea-ice by satellites present a challenge for
278 us to validate ERA5 clouds there.



279

280 **Fig. 2.** (a, b) ERA5 and (c, d) CERES total cloud fraction averaged over years 2001-2020 for (a,
 281 c) October-March and (b, d) April-September. The black contour represents the mean 15% sea-
 282 ice concentration based on ERA5 data. The MODIS clouds used in CERES likely underestimate
 283 cloud amount by 10-20% over the polar ice cap, especially during the polar night (Liu et al. 2010).



284

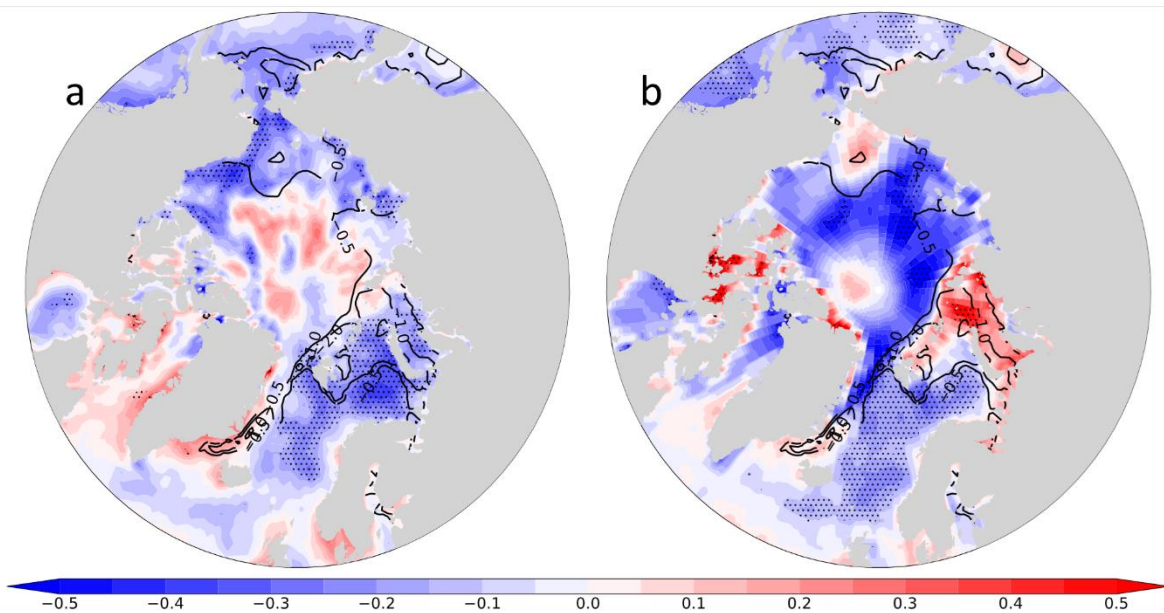
285 **Fig. 3.** Seasonal cycle (years 2001-2020) of (a, b) cloud fraction (in %), (c, d) net TOA cloud
 286 radiative effect (in W m^{-2}), and (e, f) net surface cloud radiative effect (in W m^{-2}) for CERES
 287 (black lines) and ERA5 (red lines) data averaged over ocean surfaces with (a, c, e) mean sea-ice
 288 concentration $\geq 15\%$ or (b, d, f) mean sea-ice concentration $< 15\%$. The MODIS clouds used in
 289 CERES significantly underestimate cloud amount over sea ice during the polar night (Liu et al.
 290 2010), which contributes to the low cloud fraction from November-April shown in (a).

291

292 As stated above, clouds play an important role in the Arctic TOA and surface energy
 293 balances. Figure 3c-3f shows the mean seasonal cycle of the net CRF averaged over regions with
 294 15% or greater mean SIC or regions with less than 15% SIC (excluding land) at the TOA and
 295 surface. Despite the differences in mean cloud fraction (Fig. 3a-b), ERA5 and CERES show good
 296 agreement for the TOA and surface CRF with negative CRF (of 20-100 W m^{-2}) during April-
 297 September (i.e., the sunlit months) and positive CRF (up to 50 W m^{-2}) from October-March (i.e.,

298 polar night) (Fig. 3c-f). ERA5 and CERES show a larger negative CRF over open-water surfaces
299 (Fig. 3d, f) than ice-covered surfaces (Fig. 3c, e) for both the TOA (Fig. 3d) and surface CRF (Fig.
300 3f) in June-July-August due to the larger albedo differences between the water surfaces and clouds.
301 In other words, the cloud albedo effect is more effective over dark water surfaces than over
302 reflective ice surfaces because most sunlight under clear skies would be reflected by sea ice
303 without clouds, but it would be absorbed by dark water surfaces. The TOA CRF is similar in ERA5
304 and CERES from October-March with a value of $\sim 15 \text{ W m}^{-2}$ over the Arctic (Fig. 3d) and ice-
305 covered surfaces (Fig. 3e) and $\sim 20\text{-}30 \text{ W m}^{-2}$ over ocean water surfaces (Fig. 3f). The cold-season
306 CRF warms the surface by $\sim 30\text{-}40 \text{ W m}^{-2}$ in CERES and ERA5 over ice-covered surfaces (Fig.
307 3e), and $\sim 50 \text{ W m}^{-2}$ over open-water surfaces (Fig. 3f).

308 Lastly, we examine the 2001-2020 trend maps of ERA5 (Fig. 4a) and CERES (Fig. 4b)
309 cloud fraction. Statistically significant negative cloud fraction trends occurred in the Norwegian
310 Sea for both ERA5 (Fig. 4a) and CERES (Fig. 4b) during October-March. A discrepancy in the
311 ERA5 and CERES cloud fraction trends occurred over the Barents-Kara and Chukchi Seas, with
312 decreasing clouds in ERA5 and increasing clouds in CERES. Over most of the Central Arctic
313 Ocean, cloud fraction trends were statistically insignificant at the 0.05 level in ERA5 and CERES
314 in autumn and winter (Fig. 4). The short 20-year record of CERES data or differences in cloud
315 fraction vertical profiles may account for the discrepancies between the 2001-2020 ERA5 and
316 CERES total cloud fraction trend maps.



317

318 **Fig. 4.** October-March linear trend maps for (a) ERA5 and (b) CERES total cloud fraction (in %
319 yr⁻¹; shading) and ERA5 sea-ice concentration (in % yr⁻¹; contours) for years 2001-2020.
320 Statistically significant cloud fraction trends at the 0.05 level are stippled.

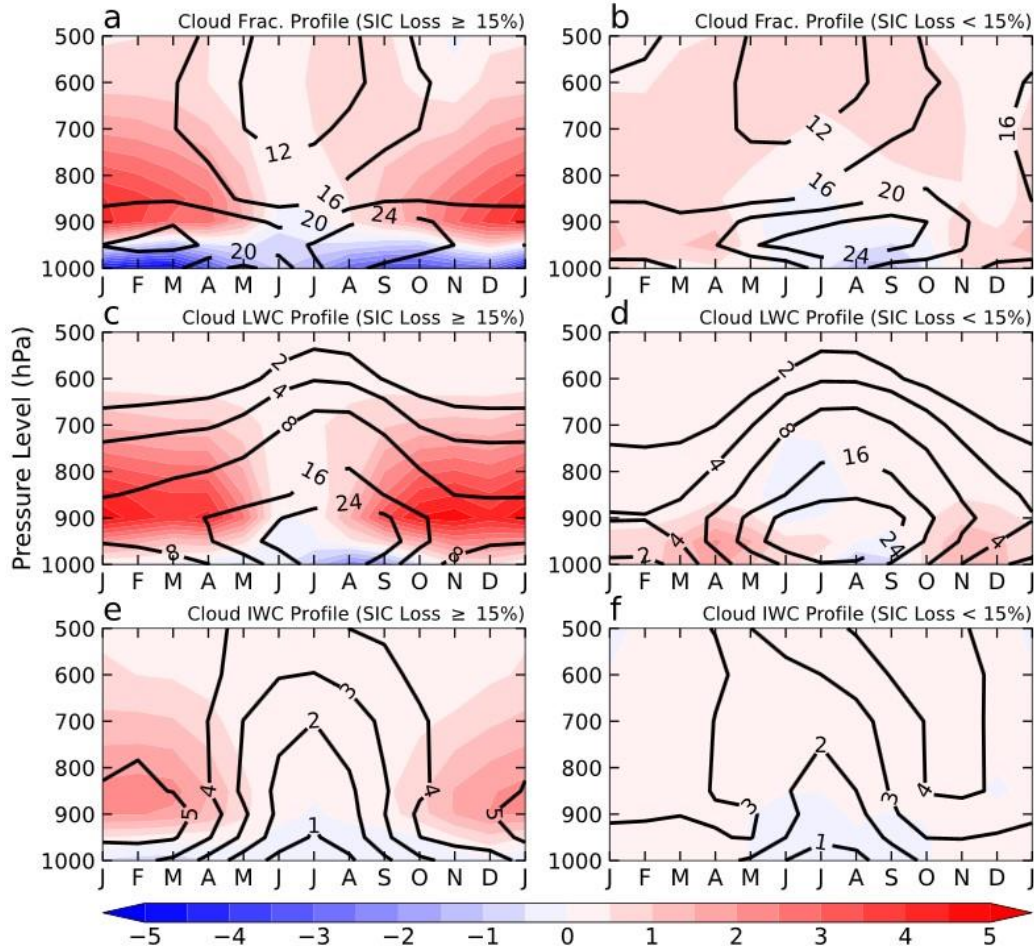
321 Our comparison of the ERA5 and CERES cloud fraction data shows that ERA5 simulates
322 the cloud fraction well over open-water surfaces during 2001-2020 (Fig. 1b) but show higher cloud
323 fraction in sea ice-covered regions with reduced seasonal variations than CERES (Fig. 2),
324 consistent with Yeo et al. (2022). The strong agreement between ERA5 and CERES cloud fraction
325 averaged over open-water surfaces suggests that ERA5 may be able to capture the cloud response
326 to sea-ice loss because melting sea ice exposes more ocean waters. We emphasize that while Arctic
327 cloud data in ERA5 contains mean biases relative to CERES, which likely underestimates cloud
328 fraction over ice-covered areas (Liu et al. 2010), the main goals of this paper are to further reveal
329 and understand the processes leading to the enhanced cloud amount over regions with sea-ice loss.
330 Thus, any mean biases over the ice surfaces in ERA5 cloud data may not change our conclusions
331 qualitatively. The underestimation of clouds over sea ice in CERES data does not necessarily
332 suggest that ERA5 overestimates clouds over sea ice-covered areas. As the ice-covered areas
333 mainly include regions around the North Pole where atmospheric conditions (e.g., stability) are
334 quite different from those near the marginal ice zone (where long-term sea-ice loss occurs), such
335 opposite differences between ice-covered and open-water surfaces do not necessarily reflect the
336 cloud response to sea-ice loss along the marginal ice zone, which is the focus of our subsequent
337 analysis. Lastly, we note that the main source of difference between ERA5 and CERES total cloud
338 fraction likely comes from low clouds over sea ice as ERA5 reasonably reproduces medium and
339 high cloud fractions in the Arctic region (Yeo et al. 2022). The lack of ground-based in-situ
340 observations and limitations of remote sensing techniques makes evaluation of ERA5 clouds
341 challenging in the Arctic.

342 **4. Climatology and long-term changes in ERA5 cloud properties**

343 We examine the 1950-1979 climatology and long-term changes (i.e., years 1990-2019
344 minus years 1950-1979) in ERA5 cloud fraction, and specific cloud liquid and ice water contents
345 for regions that experienced significant ($\geq 15\%$) or little ($< 15\%$) sea-ice loss. Figure 5a shows that
346 from 1950-1979 to 1990-2019, ERA5 cloud fraction increased by ~5-6% around 950-700 hPa but
347 decreased by similar amounts near the surface (1000-950 hPa) from October-March over regions
348 with significant sea-ice loss (mainly around the marginal ice zones, Fig. 6d). Changes in Arctic

349 cloud amount were small from May-August throughout the entire vertical profile (Fig. 5a, b), or
350 above 700 hPa (Fig. 5a) and over oceanic regions with little sea-ice loss (Fig. 5b) throughout the
351 year. The oceanic regions with little sea-ice loss include both open-water surfaces and ice-covered
352 areas well below the ice melting temperature (Fig. 6d). We notice that areas with little sea-ice loss
353 experienced slight increases in cloud fraction over the Central Arctic (i.e., ~1-3%) and decreases
354 in cloud fraction in the Norwegian and Barents Sea areas from October-March (Fig. 5d). To
355 examine the effects of the large decrease in North Atlantic clouds on Arctic mean cloud changes,
356 we average Arctic cloud properties over 55°-70°N to exclude the Central Arctic region, which is
357 mostly ice-covered through the winter season (Fig. 2a). We found that our results in Fig. 5a-c are
358 not qualitatively impacted by excluding the Central Arctic from the domain (not shown).

359 Mean cloud liquid water content (LWC) was largest from May-August near 950 hPa over
360 both areas with and without large sea-ice loss and was smaller from October-March (Fig. 5c-d). In
361 contrast, the mean cloud ice water content (IWC) was largest from December-March, especially
362 over areas with significant sea-ice loss (Fig. 5e), but was negligible in summer, likely due to
363 seasonal changes in air temperature and phase of cloud droplets. Over areas with significant sea-
364 ice loss, cloud LWC increased by $\sim 3-7 \times 10^{-3} \text{ g kg}^{-1}$ ($\sim 37.5\%$ of the 1950-1979 mean; Fig. 5c) and
365 cloud IWC increased by $\sim 1-3 \times 10^{-3} \text{ g kg}^{-1}$ ($\sim 26.7\%$; Fig. 5e) around 950-700 hPa during October-
366 March. Thus, cloud LWC increased more than cloud IWC in absolute and relative values in autumn
367 and winter from 1950-1979 to 1990-2019. Changes in cloud LWC (Fig. 5d) and IWC (Fig. 5f)
368 were negligible during summer, over areas with little sea-ice loss, and near the surface.



369

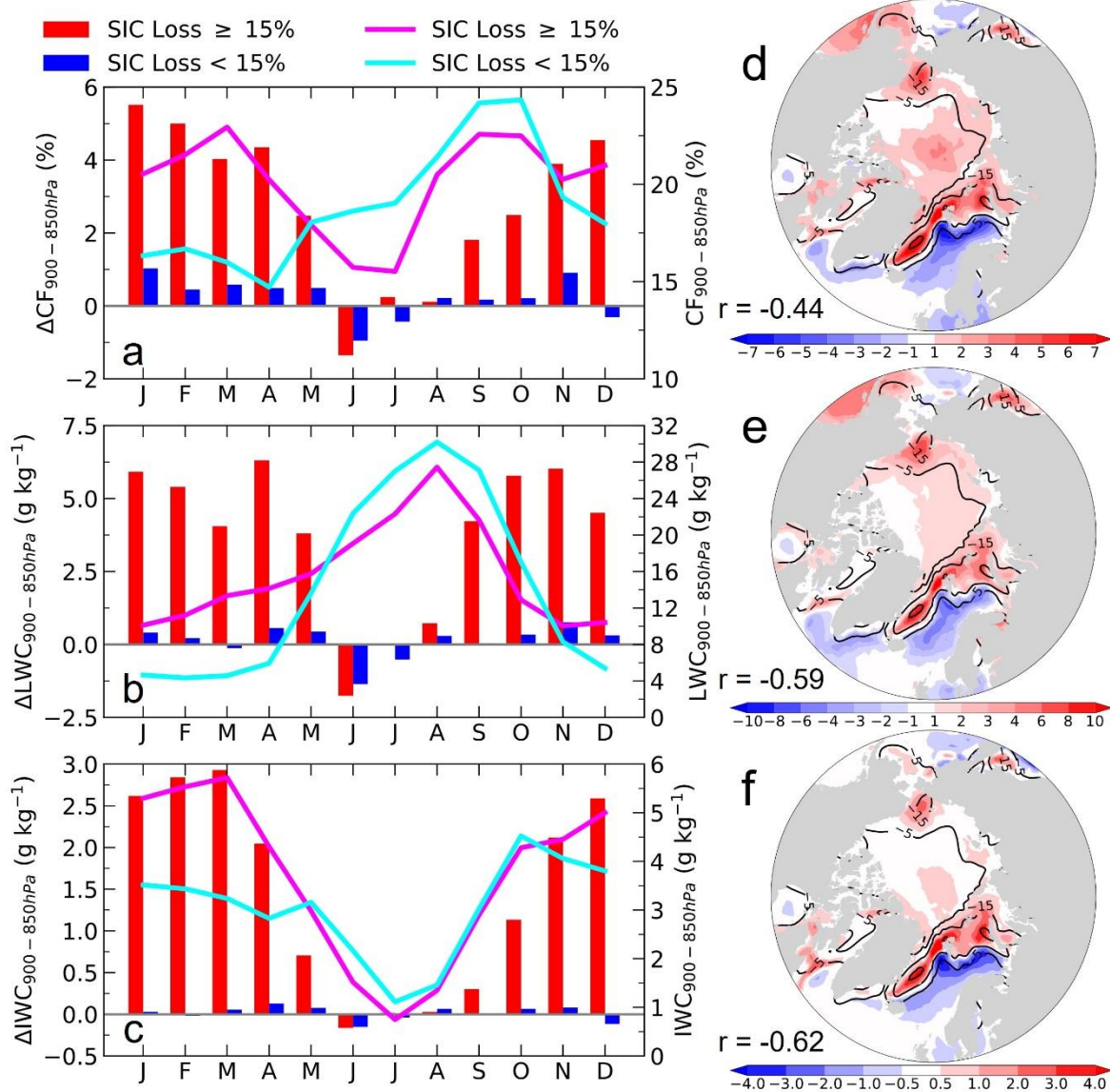
370 **Fig. 5.** Arctic (67° - 90° N) monthly mean climatology for years 1950-1979 (contours) and long-
 371 term changes (years 1990-2019 minus 1950-1979, shading) as a function of months and pressure
 372 levels in ERA5 (a, b) cloud fraction (in %), (c, d) specific cloud liquid water content (LWC, in
 373 mg kg^{-1}), and (e, f) specific cloud ice water content (IWC, in mg kg^{-1}) averaged over the oceanic
 374 areas (a, c, e) with 15% or greater SIC loss, and (b, d, f) with less than 15% SIC loss.

375

376 Changes in Arctic cloud fraction (Fig. 6a), LWC (Fig. 6b), and IWC (Fig. 6c) averaged
 377 over 900-850 hPa were greatly enhanced over areas with significant sea-ice loss compared to
 378 regions with little sea-ice loss from October-April. Specifically, the October-April Arctic cloud
 379 fraction, LWC, and IWC increased by ~ 4 - 6% of the sky, ~ 5.0 - $7.5 \times 10^{-3} \text{ g kg}^{-1}$ ($\sim 46.2\%$ of the
 380 1950-1979 mean), and ~ 2 - $3 \times 10^{-3} \text{ g kg}^{-1}$ ($\sim 47.1\%$ of the 1950-1979 mean), respectively, over
 381 areas with significant sea-ice loss. Note that the 1950-1979 mean cloud LWC (Fig. 6b) and IWC
 382 (Fig. 6c) showed a similar seasonal cycle over areas with and without significant sea-ice loss, with
 383 cloud LWC peaking in summer and IWC peaking in winter. The 1950-1979 climatology of the

384 cloud fraction averaged over 900-850 hPa showed surface dependence mainly during January-
385 April, with a maximum cloud fraction (~20-25%) from October-March over areas with significant
386 sea-ice loss and peak cloud fractions (~25%) in September and October in regions with little sea-
387 ice loss (Fig. 6a). Spatially, the long-term changes in October-March cloud fraction (Fig. 5d), cloud
388 LWC (Fig. 6e), and IWC (Fig. 6f) are moderately correlated with sea-ice loss with correlation
389 coefficients of -0.44, -0.59, and -0.62, respectively. Increases in cold season cloud properties were
390 largest off the East Coast of Greenland, in the Barents-Kara Seas, the Chukchi Sea, and the Sea of
391 Okhotsk, where there was significant SIC loss. This suggests that sea-ice loss is a major control
392 on Arctic cloud changes, but we recognize that the correlation coefficient does not imply causal
393 relationships between sea ice and cloud properties.

394 Our analysis of the vertical profiles (Fig. 5), seasonal cycles (Fig. 6a-c), and spatial
395 distributions (Fig. 6d-f) of Arctic cloud changes between 1950-1979 and 1990-2019 suggest that
396 sea-ice loss can greatly influence Arctic cloud property changes. Cloud fraction, cloud LWC and
397 IWC increased around ~950-700 hPa over regions with significant sea-ice loss from September-
398 May. From June-August and over areas with little sea-ice loss, changes in cloud properties were
399 negligible. We also found decreased Arctic cloud fraction over regions with significant sea-ice
400 loss around 1000-950 hPa mainly from August-May (Fig. 5a). Spatially, the changes in Arctic
401 cloud properties from 900-850 hPa were moderately correlated with sea-ice loss from 1950-1979
402 to 1990-2019 during October-March, with the largest changes off the East Coast of Greenland, in
403 the Barents-Kara Seas, the Chukchi Sea, and the Sea of Okhotsk, where there was more than 15%
404 sea-ice loss. In the next section, we analyze specific dynamic and thermodynamic mechanisms
405 that may link sea-ice loss to changes in the vertical profiles, seasonal cycles, and spatial patterns
406 of Arctic cloud properties.



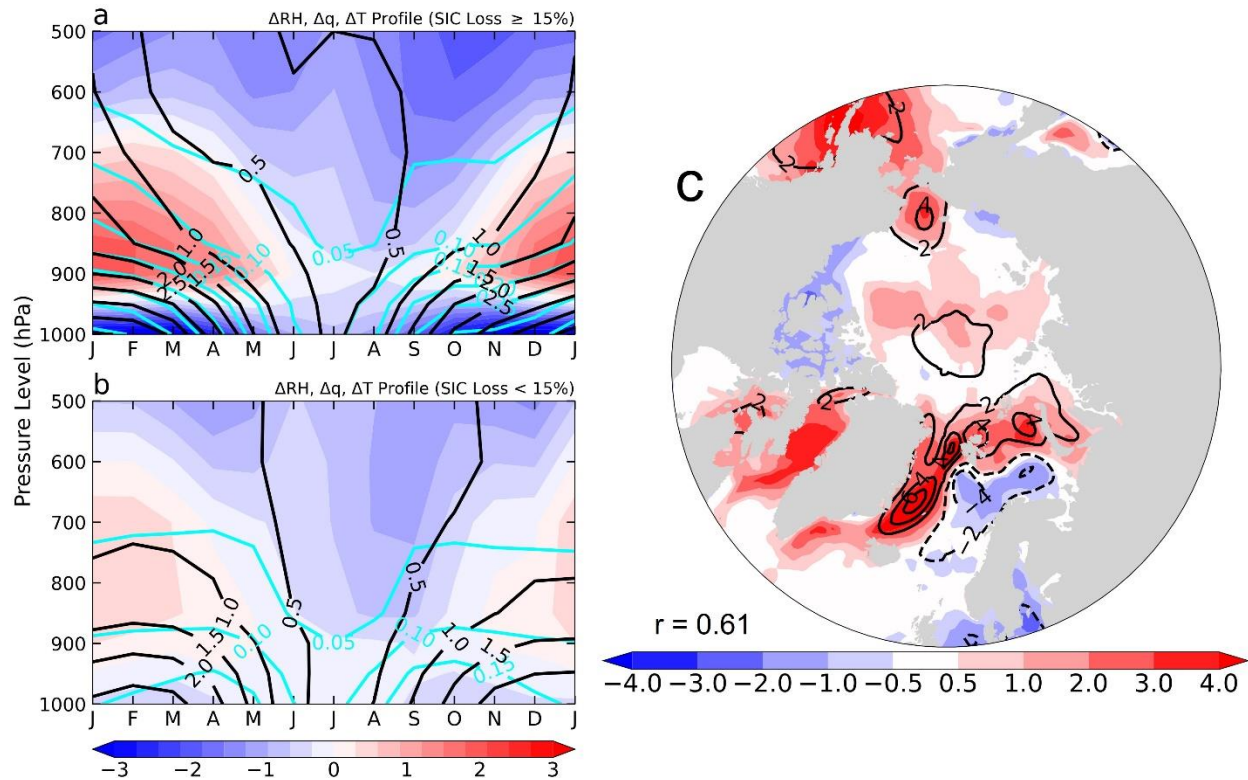
407

408 **Fig. 6.** (a-c) Long-term changes (bars; left y-axis; years 1990-2019 minus years 1950-1979) in
 409 ERA5 (a) cloud fraction (in %), (b) cloud liquid water content (in mg kg^{-1}), and (c) cloud ice water
 410 content (mg kg^{-1}) for 900-850 hPa averaged over areas with 15% or greater SIC loss (red bars) and
 411 areas with less than 15% SIC loss (blue bars) poleward of 67°N . The corresponding 1950-1979
 412 mean seasonal cycle for each variable averaged over areas with SIC loss $\geq 15\%$ (pink line), and
 413 areas with SIC loss $< 15\%$ (cyan line) is shown on the right y-axis. (d-f) Long-term changes in
 414 ERA5 October-March sea-ice concentration (shown as contours in d-f, with contour levels at -5, -
 415 15, and -30), (d) cloud fraction (shading; in %), (e) cloud liquid water content (shading; in mg kg^{-1})
 416 and (f) cloud ice water content (shading; in mg kg^{-1}) for 900-850 hPa. The corresponding pattern
 417 correlation between the shaded and contour field is shown in the bottom-left corner of (d-f). Each
 418 correlation coefficient has a p -value less than 0.01. For panels a-c, changing the averaging domain
 419 to $55^\circ\text{-}70^\circ\text{N}$ to exclude the polar ice-cap, which is a major part of the area with $<15\%$ SIC loss,
 420 does not alter the results qualitatively.

421 **5. Mechanisms linking increased Arctic cloud fraction and water content to sea-**
422 **ice loss**

423 Increased relative humidity (RH) implies that the air has moved closer to saturation,
424 favoring cloud formation. Figure 7a shows that over areas with significant sea-ice loss, RH
425 increased by ~2-4% between 950-700 hPa but decreased by more than 4% from 1000-950 hPa
426 during October-March. This is consistent with the increased cloud fraction between 950-700 hPa
427 and decreased cloud fraction between 1000-950 hPa over areas with significant sea-ice loss (Fig.
428 5a). A slight RH increase (<1%) occurred over regions with little sea-ice loss between 950-700
429 hPa (Fig. 7b). The RH profile changed little from May-August over regions with and without sea-
430 ice loss. Spatially, changes in RH around 900-850 hPa are strongly correlated with cloud fraction
431 changes ($r = 0.61$) around 900-850 hPa. We found that cloud fraction increased by ~2-4% in the
432 Norwegian Sea, Barents-Kara Seas, and Chukchi Sea where RH increased. Further, the RH around
433 900-850 hPa decreased near the coast of Norway and Sweden in the North Atlantic Ocean, which
434 may partially explain suppressed cloud fraction (Fig. 6d, 7c), and cloud LWC (Fig. 6e) and IWC
435 (Fig. 6f) in this area. We note that more work is required to understand this slight decrease in cloud
436 fraction and water content in the Atlantic sector and is not the focus of this study.

437 Figure 7a shows that the changes in air temperature and specific humidity over areas with
438 significant sea-ice loss were largest from October-March near the surface and they weakened with
439 height, consistent with the bottom-heavy warming profiles for the Arctic cold season shown
440 previously (Jenkins and Dai 2022). Atmospheric warming and moistening were weak from May-
441 August and over areas with little sea-ice loss (Fig. 7b). The large warming from 1000-950 hPa
442 over regions with significant sea-ice loss increased the saturation specific humidity and thus
443 decreased the RH and cloud fraction there. From 950-700 hPa, the effect of atmospheric
444 moistening outpaced the effect of warming, leading to increased RH and thus cloud fraction.
445 Enhanced vertical motions over areas with significant sea-ice loss (e.g., Fig. 10a) transport
446 moisture away from the near-surface layer to the layer around 950-700 hPa, decreasing
447 (increasing) the RH near the surface (around 950-700 hPa). The lack of strong warming and
448 moistening during the summer months produces small (i.e., <1%) RH changes (Fig. 7a), thus
449 resulting in small changes in cloud properties during the warm season (Fig. 6a-c).



450

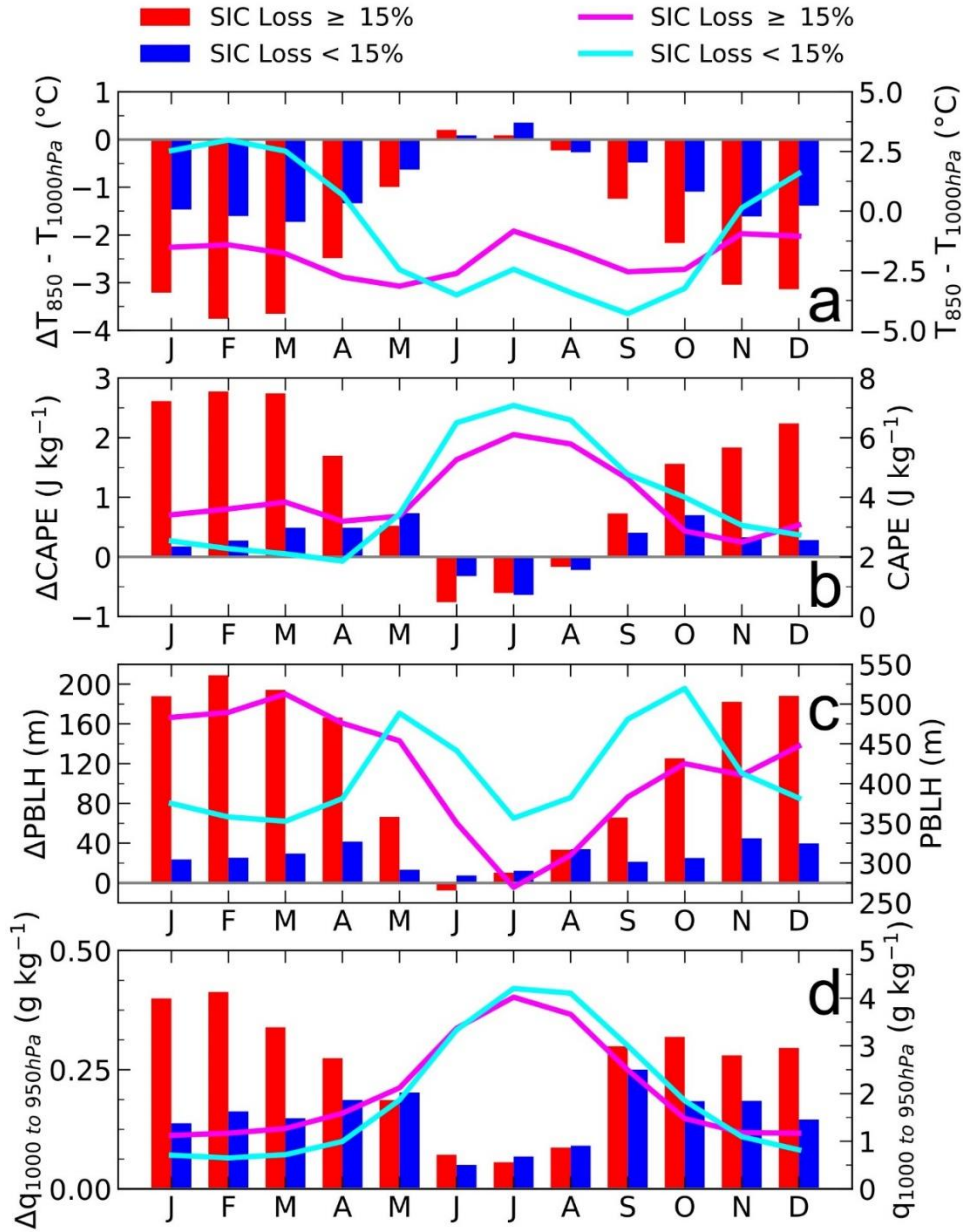
451 **Fig. 7.** Arctic (67° - 90° N) monthly mean changes (years 1990-2019 minus years 1950-1979) in
 452 ERA5 relative humidity (%; shading), specific humidity (g kg^{-1} ; cyan contours), and air
 453 temperature ($^{\circ}\text{C}$; black contours) averaged over the oceanic areas with (a) SIC loss $\geq 15\%$ and (b)
 454 SIC loss $< 15\%$. (c) Changes in relative humidity (%; shading) and cloud fraction (%; contours)
 455 averaged over 900-850 hPa. The pattern correlation between the shaded and contour fields is
 456 shown in the bottom corner of (c).

457

458 Figure 8a shows the 1950-1979 climatology and long-term changes of the Arctic lower
 459 tropospheric temperature inversion (i.e., $T_{850 \text{ hPa}} - T_{1000 \text{ hPa}}$). We note that the $T_{850 \text{ hPa}} - T_{1000 \text{ hPa}}$
 460 inversion in ERA5 is underestimated relative to observations, but that ERA5 reproduces the
 461 general structure of the Arctic temperature profile well (Graham et al. 2019a) and simulates
 462 atmospheric conditions better than other reanalysis datasets (Graham et al. 2019b). Arctic mean
 463 temperature profile is stable with a temperature inversion over areas with little sea-ice loss from
 464 November-April. A stable profile with a strong lower-tropospheric temperature inversion would
 465 suppress vertical mixing between the surface and lower troposphere and result in weak vertical
 466 transfer of moisture and energy. From 1950-1979 to 1990-2019, the strength of the Arctic lower
 467 tropospheric temperature inversion decreased in all but the summer months, especially over
 468 regions with significant sea-ice loss (Fig. 8a). This suggests that enhanced surface warming

469 induced by sea-ice loss weakens Arctic lower tropospheric stability, thus favoring an environment
470 for enhanced vertical motion and mixing. To demonstrate that, we further show the climatology
471 and changes in convective available potential energy (CAPE; Fig. 8b) and planetary boundary
472 layer height (PBLH; Fig. 8c) over the Arctic. The 1950-1979 CAPE climatology shows a similar
473 seasonal cycle with peak positive CAPE in summer over areas with and without significant sea-
474 ice loss. CAPE increased by $\sim 2\text{--}2.75 \text{ J kg}^{-1}$ ($\sim 100\%$ of the 1950-1979 climatology) from October-
475 March over areas with significant sea-ice loss, compared to a less than 1 J kg^{-1} increase over areas
476 with little sea-ice loss (Fig. 8b). The PBLH increase was also largest ($\sim 120\text{--}200 \text{ m}$) from October-
477 March over areas with significant sea-ice loss (Fig. 8c). The reduced temperature inversion,
478 increased CAPE, PBLH, and near-surface specific humidity (Fig. 8d) over areas with significant
479 sea-ice loss suggest that warming associated with Arctic sea-ice loss increased vertical transport
480 of moisture and energy from the surface layer to lower troposphere, favoring increased RH and
481 enhanced cloud formation from $\sim 950\text{--}700 \text{ hPa}$.

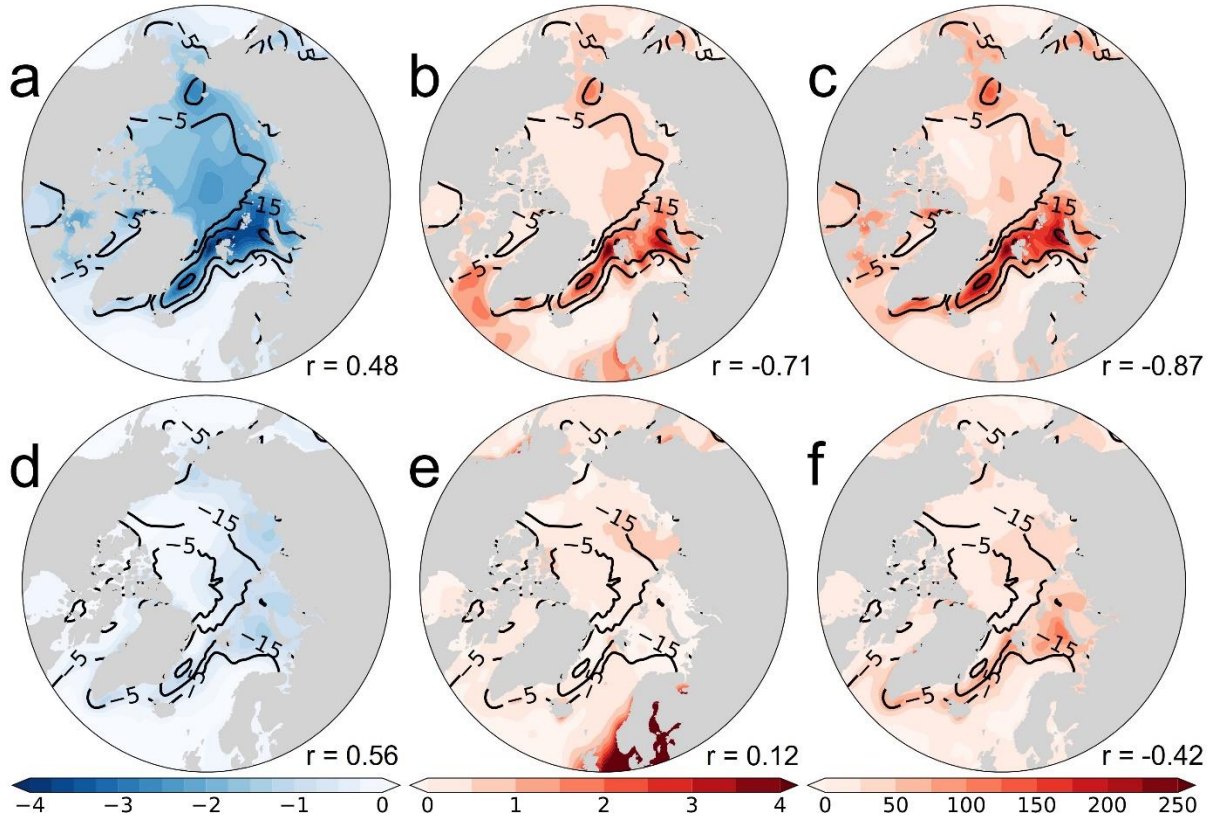
482 The spatial distributions of the October-March CAPE (Fig. 9b) and PBLH (Fig. 9c)
483 changes correspond strongly to the patterns of sea-ice loss with correlation coefficients -0.71 , and
484 -0.87 , respectively. The temperature inversion change patterns were also correlated with the sea-
485 ice loss ($r = 0.48$, Fig. 9a). Over areas with significant sea-ice loss, the temperature inversion
486 weakened by $-3\text{--}4 \text{ }^\circ\text{C}$ and slightly decreased by $-1\text{--}2 \text{ }^\circ\text{C}$ over the Central Arctic region where
487 less than 5% SIC loss occurred (Fig. 9a). Similarly, changes in cold-season CAPE (Fig. 9b) and
488 PBLH (Fig. 9c) were localized over areas with large sea-ice loss, with the largest increases near
489 the East Coast of Greenland, the Barents-Kara Sea, the Sea of Okhotsk, and Chukchi Sea. The
490 temperature inversion changed little during April-September but exhibited a moderate pattern
491 correlation with sea-ice loss ($r = 0.56$; Fig. 9d). Further, the April-September spatial patterns of
492 CAPE (Fig. 9e) and PBLH (Fig. 9f) changes were weakly correlated with sea-ice changes, with
493 correlation coefficients of 0.12 and -0.42 , respectively. Our analyses suggest that sea-ice loss,
494 which enhances winter surface warming (Deser et al. 2010; Dai et al. 2019), can lead to reduced
495 temperature inversion, increased vertical mixing, and higher CAPE and PBLH from October-
496 March, while the influence is small in the warm season.



497

498 **Fig. 8.** Long-term changes (bars, left y-axis; years 1990-2019 minus 1950-1979) in ERA5 (a) T_{850}
 499 hPa minus $T_{1000 \text{ hPa}}$ difference (in $^{\circ}\text{C}$), (b) convective available potential energy (CAPE; in J kg^{-1}),
 500 (c) planetary boundary layer height (PBLH; in m), and (d) 1000 hPa to 950 hPa mean specific
 501 humidity (in g kg^{-1}) averaged over regions with 15% or greater SIC loss (red bars) and regions
 502 with less than 15% SIC loss (blue bars) poleward of 67°N . The corresponding 1950-1979 mean
 503 seasonal cycle for each variable averaged over areas with 15% or greater SIC loss (red line), and
 504 areas with less than 15% SIC loss (blue line) is shown on the right y-axis.

505

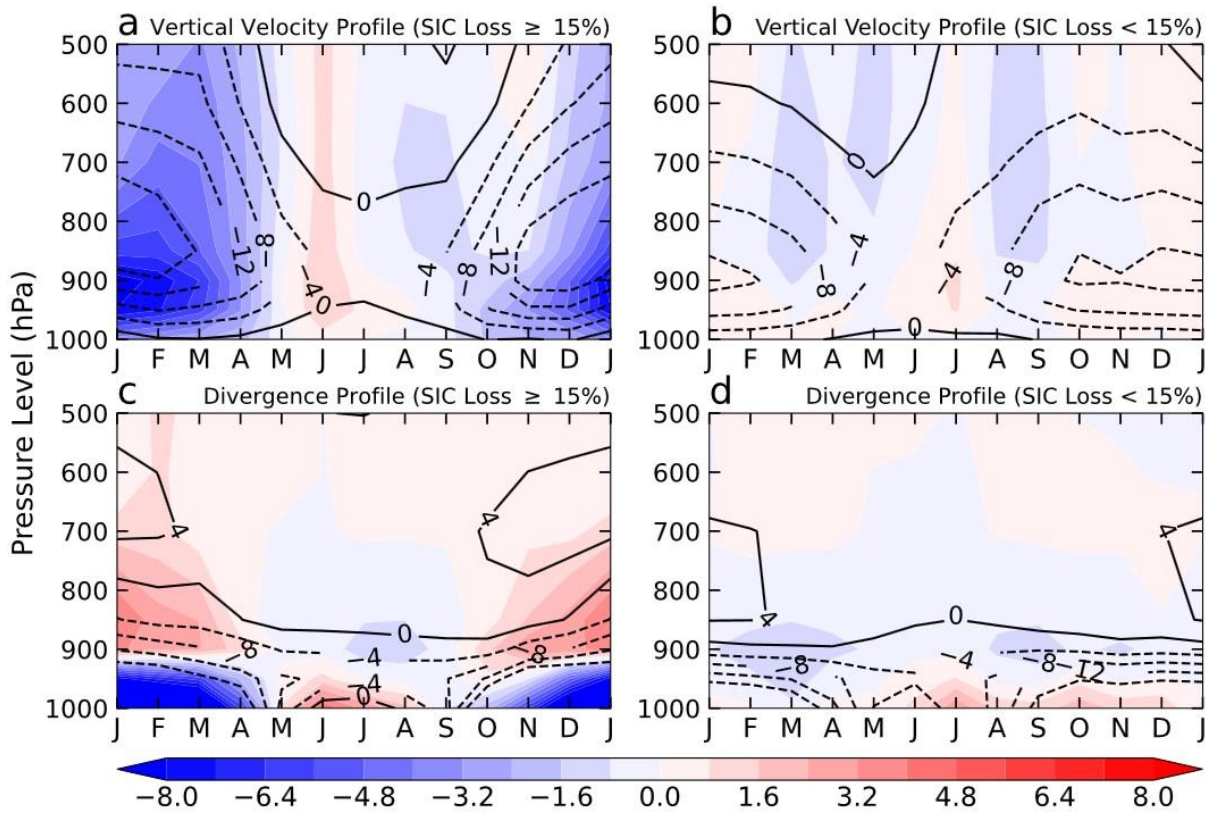


506

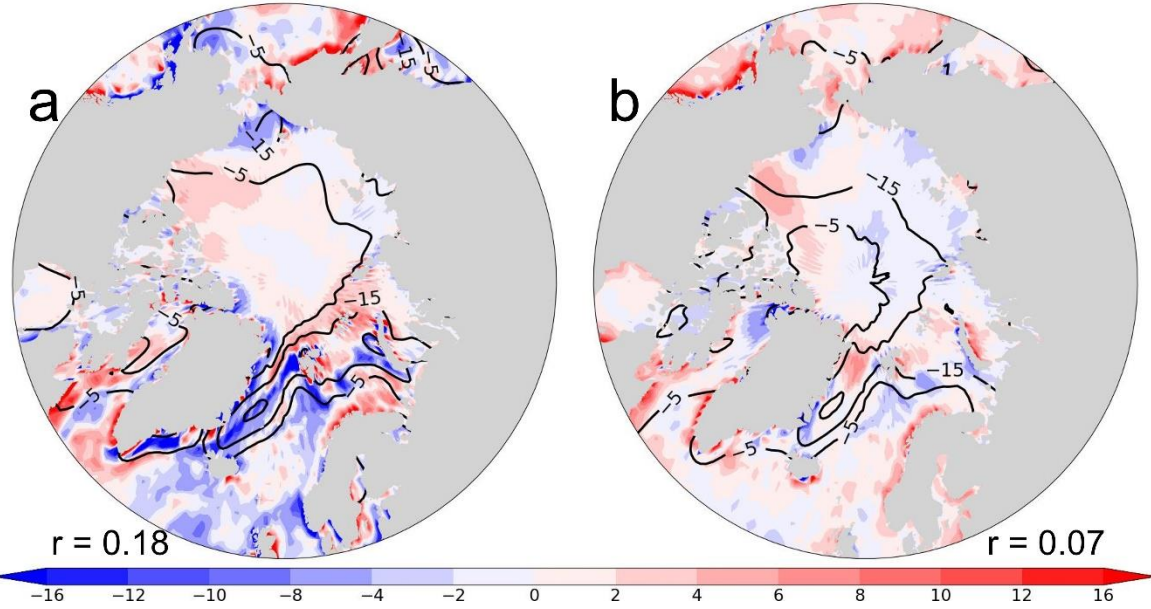
507 **Fig. 9.** Long-term changes (years 1990-2019 minus years 1950-1979) in ERA5 sea-ice
 508 concentration (contours; %; the -5, -15, and -30% levels are shown) and (a, d) $T_{850 \text{ hPa}} - T_{1000 \text{ hPa}}$
 509 difference (shading; $^{\circ}\text{C}$), (b, e) CAPE (shading; J kg^{-1}), and (c, f) PBLH (shading; m) for (a-c)
 510 October-March and (d-f) April-September. The pattern correlation between the shaded and contour
 511 field is shown in the bottom-right corner of each panel. All the correlation coefficients have a p -
 512 value less than 0.01.

513 Figure 10 shows the climatology and changes in the profiles of vertical velocity and
 514 horizontal wind divergence. The 1950-1979 mean vertical velocity was upward from October-
 515 March, with a magnitude of $-12 \sim -16 \text{ Pa s}^{-1}$ ($-8 \sim -12 \text{ Pa s}^{-1}$) over regions with $\geq 15\%$ ($< 15\%$) SIC
 516 loss. From May-August, the 1950-1979 mean vertical velocity was near-zero over both surface
 517 types (Fig. 10a, b). Over areas with significant sea-ice loss, upward motion was enhanced in the
 518 lower troposphere (i.e., 950-800 hPa) from October-March by $-8 \times 10^{-3} \text{ Pa s}^{-1}$, while the changes
 519 during May-September were negligible (Fig. 10a). Without significant sea-ice loss, vertical
 520 velocity changed little for all months from the surface to 500 hPa (Fig. 10b). The spatial patterns
 521 of the cold-season vertical velocity changes from 950-700 hPa show enhanced upward motion East
 522 of Greenland and in the Barents-Kara Seas, with small increases in upward motion in the Chukchi
 523 Sea (Fig. 11a). Upward vertical velocity increased most over areas with large sea-ice loss during

524 the cold season, although the two only show a weak pattern correlation ($r = 0.18$) (Fig. 11a). April-
 525 September experienced little change in vertical velocity and its changes did not spatially
 526 correspond with sea-ice loss ($r = 0.07$; Fig. 11b). The warming associated with sea-ice loss likely
 527 enhanced upward vertical motions from 1950-1979 to 1990-2019 by making the air near the
 528 surface more buoyant. Further, enhanced upward atmospheric motions over newly exposed ocean
 529 water surfaces would lead to increased upward transport of energy and moisture and enhanced
 530 cloud fraction and water content from 950-700 hPa.



531
 532 **Fig. 10.** Arctic (67° - 90° N) monthly mean climatology (years 1950-1979, contours) and changes
 533 (years 1990-2019 minus 1950-1979, shading) in ERA5 (a, b) vertical velocity (in mPa s^{-1} , negative
 534 upward) and (c, d) horizontal wind divergence (in $\text{s}^{-1} \times 10^{-7}$) averaged over the oceanic areas (a,
 535 c) with 15% or greater SIC loss and (b, d) with less than 15% SIC loss.
 536

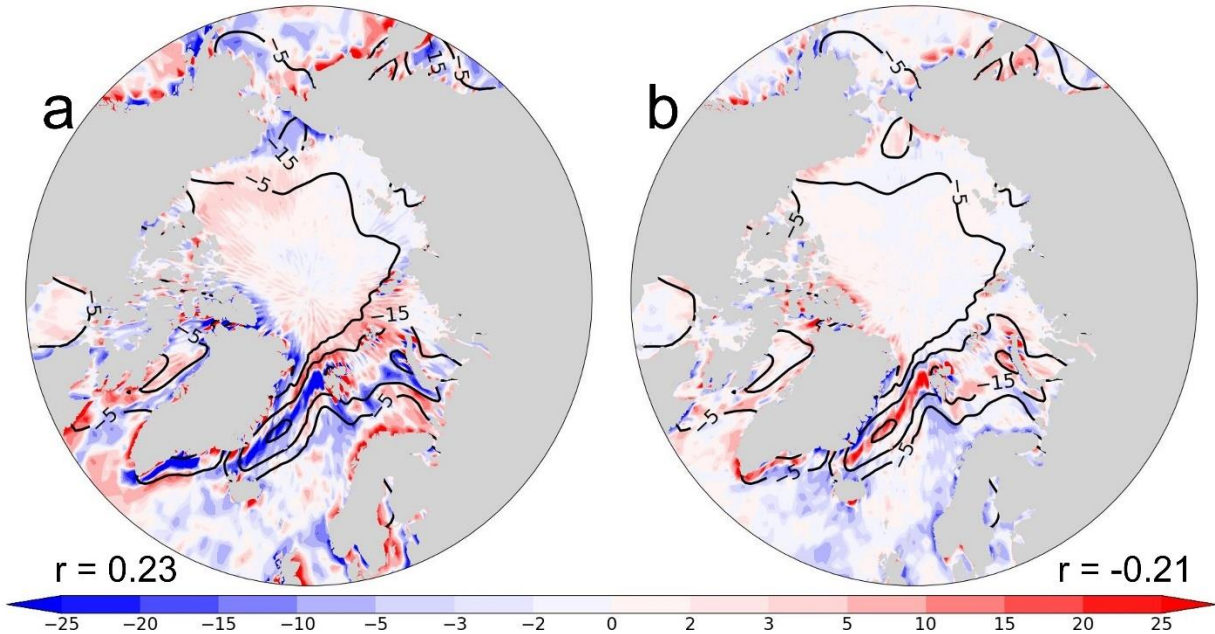


537

538 **Fig. 11.** Long-term changes (years 1990-2019 minus 1950-1979) in ERA5 vertical velocity (in
 539 mPa s^{-1} ; shading) averaged over 950-700 hPa and sea ice concentration (%; contours) for (a)
 540 October-March and (b) April-September. The pattern correlation between the divergence and sea
 541 ice change fields is shown in the bottom corner of each panel. Each correlation has a p -value less
 542 than 0.01.

543 We further examine the vertical profiles (Fig. 10c, d) and spatial patterns (Fig. 12) of
 544 horizontal wind divergence, which is related to the vertical gradient of the vertical velocity so that
 545 a horizontal convergence of airmass would lead to a vertical divergence of airmass. Over both
 546 areas with (Fig. 10c) and without (Fig. 10d) significant SIC loss, the 1950-1979 climatological
 547 conditions show mean convergence near the surface (i.e., 1000-800 hPa) and mean divergence in
 548 the layer ~ 800 -600 hPa (Fig. 10c, d), consistent with the decrease in upward velocity with height
 549 below ~ 800 hPa (Fig. 10a-d). The divergence change strongly depends on sea-ice loss. With less
 550 than 15% sea-ice loss the divergence profile experienced minimal changes throughout the year
 551 (Fig. 10d). In regions with significant SIC loss, the low-level (1000-950 hPa) convergence
 552 increased by $\sim 8 \times 10^{-7} \text{ s}^{-1}$ during October to March while the change aloft (~ 900 -700 hPa) was a
 553 divergence of $\sim 2.5 \times 10^{-7} \text{ s}^{-1}$, which weakened the mean convergence below ~ 800 hPa but enhanced
 554 the divergence above (Fig. 10c). We also note that from May-August there is a positive divergence
 555 change around 1000-950 hPa, which should weaken the climatological convergence during these
 556 months (Fig. 10c). The change patterns of the divergence fields averaged over 1000-950 hPa (Fig.
 557 12a) and 900-850 hPa (Fig. 12b) confirm that areas with 15% or greater sea-ice loss experienced

558 enhanced near-surface convergence ($r = 0.23$; Fig. 12a) and strengthened divergence aloft ($r = -$
 559 0.21 ; Fig. 12b). Note the striking alignment of the convergence (divergence) change from 1000-
 560 950 hPa (900-850 hPa) between Greenland and Svalbard.



561
 562 **Fig. 12.** Long-term changes (years 1990-2019 minus 1950-1979) in ERA5 horizontal divergence
 563 (in $\text{s}^{-1} \times 10^{-7}$; shading) averaged over (a) 1000-950 hPa and (b) 900-850 hPa for October-March.
 564 Contours represent the change in sea-ice concentration for years 1990-2019 minus years 1950-
 565 1979. The pattern correlation between the divergence and sea ice change fields is shown in the
 566 bottom corner of each panel. Each correlation has a p -value less than 0.01.
 567

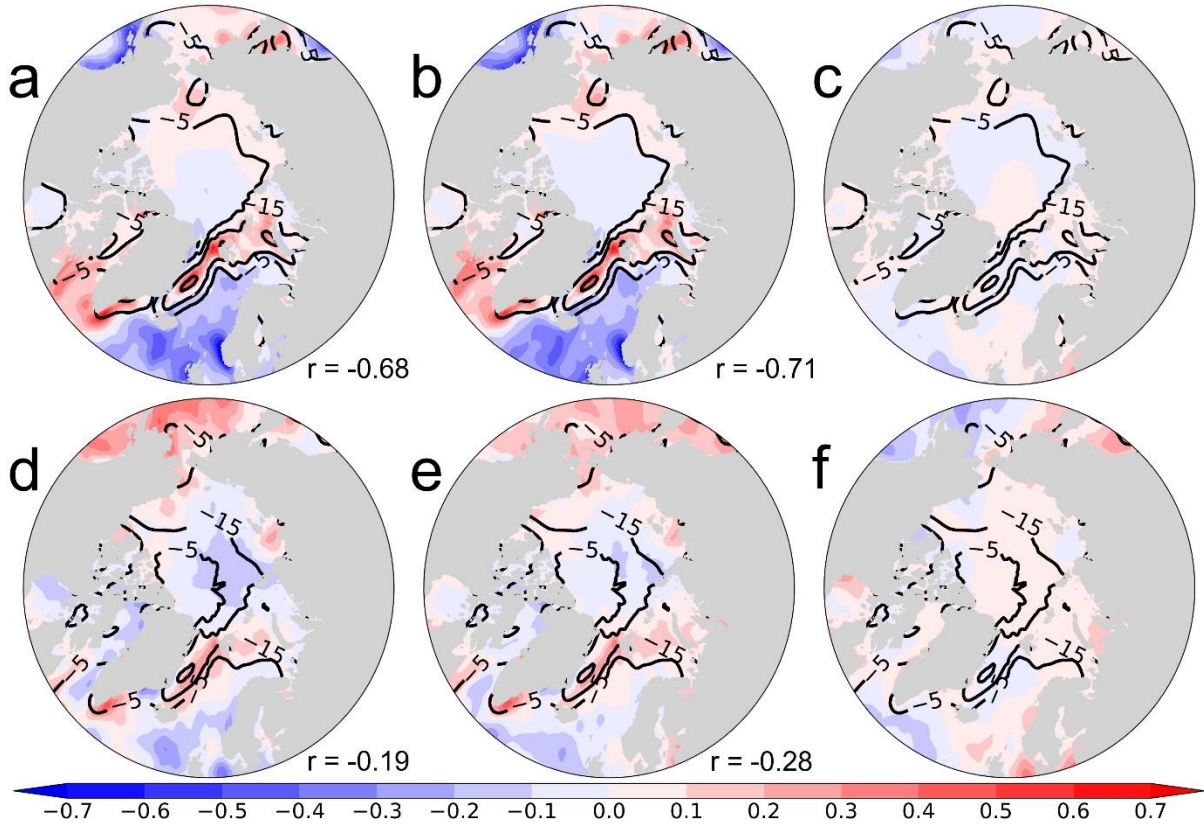
568 *b. Changes in moisture divergence, precipitation, and surface evaporation*

569 We conduct a brief analysis of the spatial patterns of the mean vertically integrated
 570 horizontal moisture divergence (Fig. 13a, d), precipitation, and surface evaporation (Fig. 14) to
 571 further reveal how sea-ice loss affects clouds through the surface water fluxes. The changes in
 572 moisture divergence exhibit strong negative spatial correlation with sea-ice changes from October-
 573 March ($r = -0.68$; Fig. 13a), but the correlation is weak from April-September ($r = -0.19$; Fig. 13d).
 574 Further, the largest increases in moisture divergence occurred over areas with 15% or greater sea-
 575 ice loss (Fig. 13a) during October-March with an increase of $0.3-0.7 \text{ mm day}^{-1}$. The enhancement
 576 of moisture divergence was largest near Greenland and Svalbard, but there were noticeable
 577 increases in moisture divergence in the Chukchi Sea and Sea of Okhotsk. This suggests that

578 atmospheric motions tended to decrease atmospheric moisture content over areas with sea-ice
579 retreat during October-March.

580 We next examine the change patterns in surface evaporation (Fig. 14a, c), precipitation
581 (Fig. 14b, d), and evaporation minus precipitation (E-P; Fig. 13 b, e), and their relationship to sea-
582 ice loss. Evaporation (Fig. 14a) and precipitation (Fig. 14b) are closely related to sea-ice loss from
583 October-March ($r = -0.87$ and $r = -0.52$). Lack of ocean-atmosphere coupling from April-
584 September produced weak or no correlation between surface evaporation ($r = -0.34$; Fig. 14c) or
585 precipitation ($r = 0.02$; Fig. 14d) and sea-ice changes. We notice that October-March precipitation
586 increases nearly everywhere under rising temperatures, with some enhancement over areas with
587 significant sea-ice loss (Fig. 14b). In contrast, changes in evaporation were localized over sea-ice
588 loss regions during October-March (Fig. 14a). E-P exhibits a strong negative correlation with sea-
589 ice loss during October-March ($r = -0.71$; Fig. 13b), but this relationship weakens from April-
590 September ($r = -0.28$; Fig. 13e). Over regions with sea-ice loss, surface evaporation exceeded the
591 total precipitation by $\sim 0.3-0.7 \text{ mm day}^{-1}$, implying net moistening of the atmosphere through
592 surface water fluxes during the cold-season in sea-ice retreat areas (Fig. 13b). The net increase in
593 surface evaporation and moisture divergence suggests that surface water fluxes, rather than remote
594 moisture transport, are a key moisture source for enhanced Arctic cloudiness during the cold
595 season. The difference between the changes in moisture flux divergence and changes in E-P fields
596 are approximately zero over most areas of the Arctic for both October-March (Fig. 13c) and April-
597 September (Fig. 13f), suggesting that net increases in surface moisture fluxes are balanced by
598 atmospheric moisture divergence, as changes in atmospheric water storage are relatively small.

599

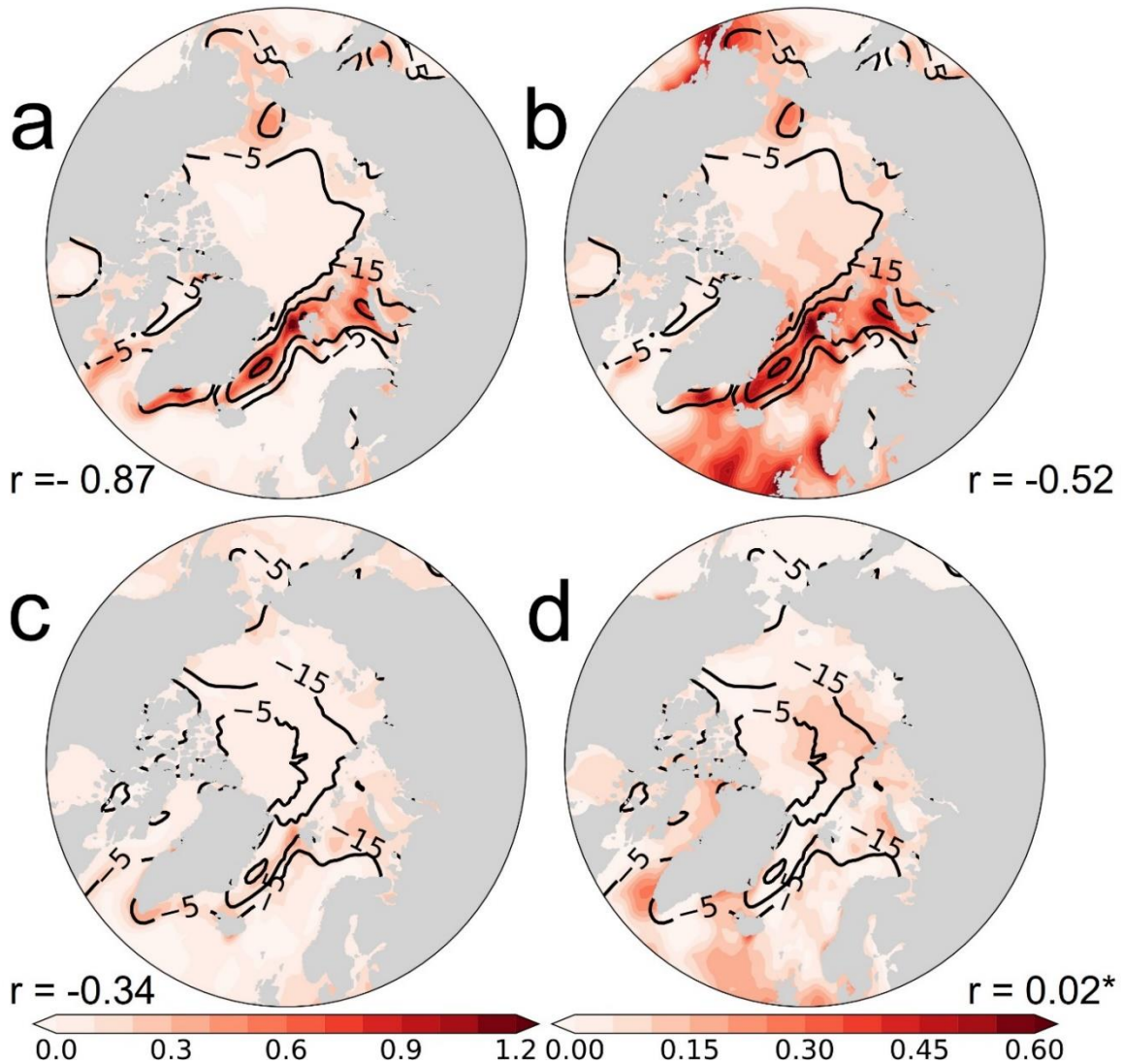


600

601 **Fig. 13.** Long-term changes (years 1990-2019 minus years 1950-1979) in ERA5 sea-ice
 602 concentration (contours; %; the -5 -15, and -30% levels are shown) and (a, d) vertically integrated
 603 atmospheric moisture flux divergence (shading; in mm day^{-1}), (b, e) evaporation minus
 604 precipitation (E - P; shading; mm day^{-1}), and (c, f) their difference for (a-c) October-March and
 605 (d-f) April-September. The pattern correlation between the shaded and contour field is shown in
 606 the bottom-right corner of (a, b, d, e). Each correlation coefficient has a p -value less than 0.01.

607

608



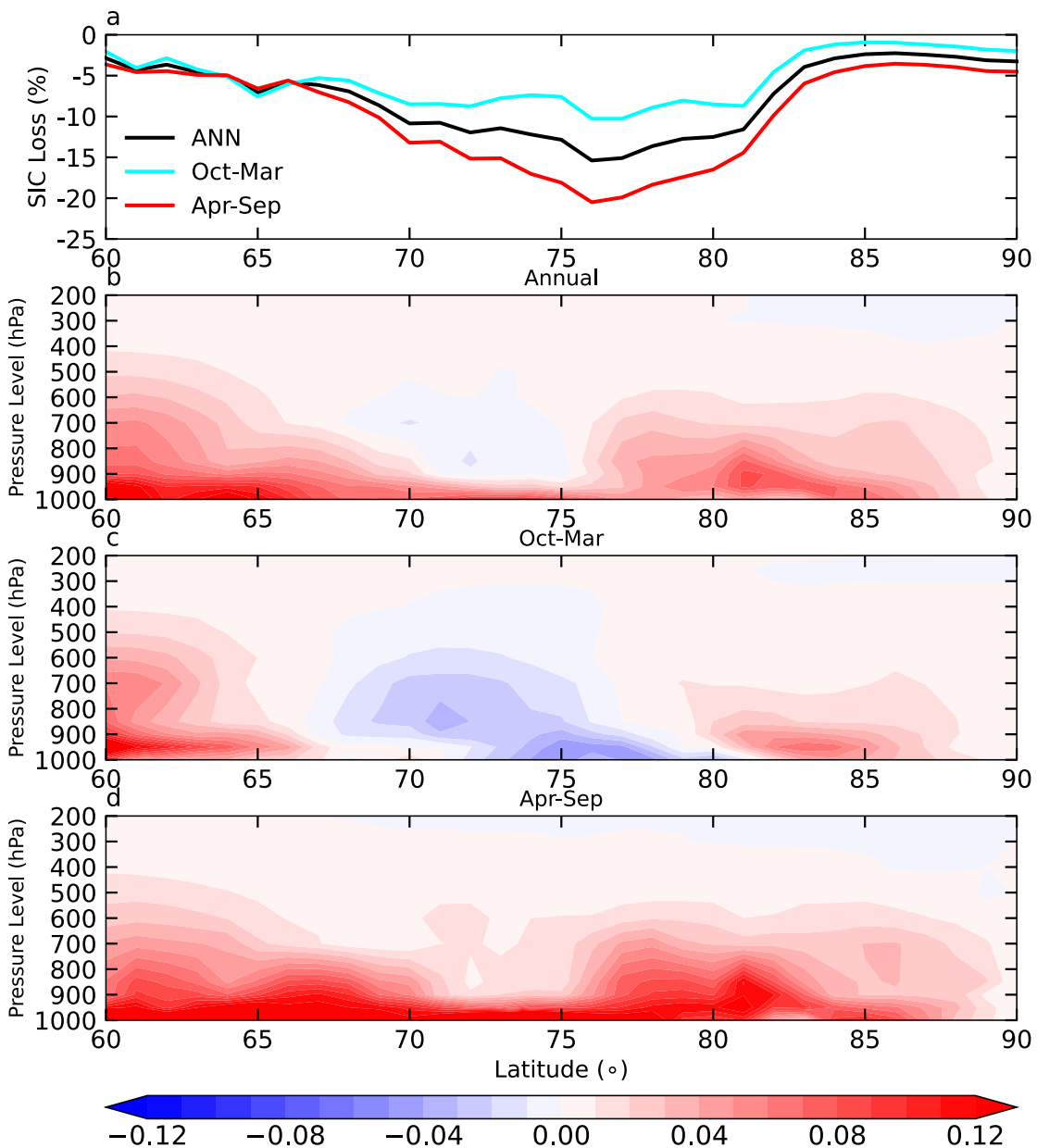
609

610 **Fig. 14.** Long-term changes (years 1990-2019 minus years 1950-1979) in ERA5 sea-ice
 611 concentration (contours; %; the -5 -15, and -30% levels are shown) and (a, c) evaporation (E;
 612 shading; left color bar; mm day^{-1}) and (b, d) precipitation (P; shading; right color bar; mm day^{-1})
 613 for (a-b) October-March and (c-d) April-September. The pattern correlation between the shaded
 614 and contour field is shown in the bottom-right corner of each panel. Each correlation coefficient
 615 has a p -value less than 0.01 except for the case in (d).

616

617 One may argue that there is a net increase in remote atmospheric moisture input into the
 618 Arctic and that the enhanced moisture is redistributed into the spatial patterns shown in Figures 13
 619 and 14. In Figures 15 and 16, we show the zonal-mean changes in meridional moisture transport
 620 (Fig. 15b-d) and vertically integrated northward water vapor flux (Fig. 16). In the annual-mean

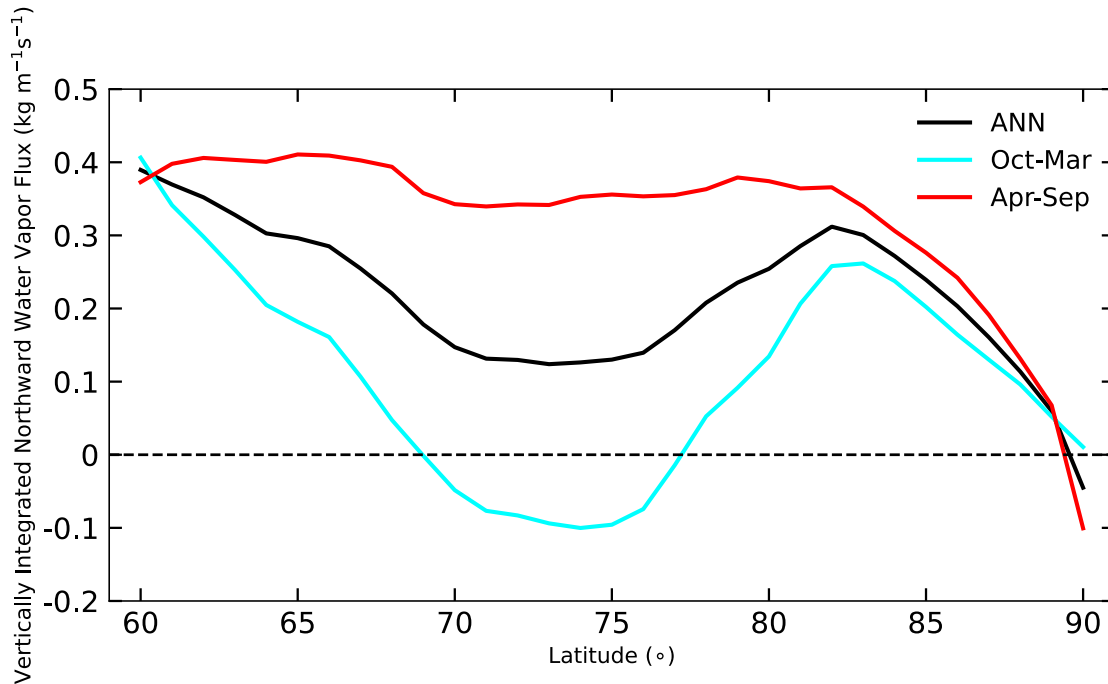
621 and from April-September, there is a net increase in meridional moisture transport at all latitudes
 622 in the Arctic (Fig. 16) from ~1000-800 hPa (Fig. 15b, d). From October-March, there is a decrease
 623 in the vertically integrated northward water vapor flux (Fig. 16) and meridional moisture transport
 624 (Fig. 15c) across ~70°-77°N, where cold season sea-ice loss is largest (Fig. 15a). Thus, remote
 625 moisture transport plays a key role in moistening the Arctic from April-September but weakens
 626 over latitudes where there is large sea-ice loss from October-March. This further suggests that
 627 enhanced evaporation from exposed water surfaces plays a key role in moistening the Arctic
 628 boundary layer in the cold season.



629

630 **Fig. 15.** Zonal-mean changes in (a) sea-ice concentration (in %), and (b-d) vertical profiles of
631 meridional moisture transport (vq ; in $\text{g kg}^{-1} \text{m s}^{-1}$) for the (b) annual, (c) October-March, and (d)
632 April-September mean.

633



634

635 **Fig. 16.** Zonal-mean change in the vertically integrated northward water vapor flux for the annual
636 (black line), October-March (cyan line), and April-September (red line) mean.

637

638 6. Summary and Discussion

639 a. Summary

640 To examine how sea-ice loss may affect clouds in the Arctic, we analyzed the long-term
641 changes from 1950-1979 to 1990-2019 in sea ice concentration (SIC), cloud fraction, cloud liquid
642 and ice water contents, and other surface and atmospheric fields using ERA5 reanalysis data. We
643 first made a comparison of ERA5 cloud fraction and cloud radiative forcing (CRF) data with
644 CERES satellite data from January 2001 to December 2020. ERA5 produces more clouds over sea
645 ice relative to satellite observations although the MODIS clouds used in CERES may be
646 underestimated, especially in winter (Liu et al. 2010). Net CRF agrees well between reanalysis and
647 CERES data; however, ERA5 radiation fields may be tuned to correct for biases or deficiencies in

648 radiation fields. We emphasize that the physical processes revealed using ERA5 data provide
649 useful insights into how sea-ice loss may influence Arctic clouds, despite the potential biases and
650 deficiencies in ERA5 cloud fields.

651 The ERA5 data show that Arctic cloud fraction, cloud liquid and ice water contents around
652 ~950-700 hPa increased from 1950-1979 to 1990-2019 over areas with significant ($\geq 15\%$) sea-ice
653 loss, while cloud fraction around 1000-950 hPa decreased during October-March. Negligible
654 changes in cloud properties occurred over areas with little ($< 15\%$) sea-ice loss or during April-
655 September. Atmospheric warming and moistening was strongest in autumn and winter near the
656 surface but was weak during summer. Large surface warming increased the saturation specific
657 humidity of the near-surface layer more than its actual specific humidity, whose rate of increase
658 may be partially counteracted by enhanced upward export of moisture. This imbalance in the rate
659 of increase between saturation and actual specific humidity resulted in a decrease in the RH and
660 cloud amount around 1000-950 hPa. From ~950-700 hPa where warming was weaker than near
661 the surface, the atmosphere experienced a net moistening (as indicated by the increased RH) likely
662 due to increased upward moisture transport, leading to enhanced cloud amount and cloud water
663 content there. The RH changed little during the summer season or over areas with little sea-ice
664 loss. During the cold season, atmospheric moisture divergence, which is a measure of surface E-P
665 flux, increased over the areas with significant sea-ice loss from 1950-1979 to 1990-2019. We also
666 show that the long-term change in meridional moisture transport is equatorward along latitudes
667 with large cold-season sea-ice loss. This suggests that increased local surface evaporation, rather
668 than remote moisture transport, provides a key moisture source for increased cloudiness over
669 newly exposed ocean water surfaces in winter.

670 *b. Discussion*

671 Our results using ERA5 data showed that sea-ice loss is associated with increased cloud
672 fraction and cloud water content during Arctic autumn and winter, consistent with previous studies
673 (e.g., Kay and Gettelman 2009; Palm et al. 2010; Morrison et al. 2019). This study makes a novel
674 contribution to this general topic by analyzing the long-term changes (i.e., the difference between
675 two 30-year periods), rather than by examining variations and trends over shorter periods (i.e., 20
676 years or less) as done previously (Schweiger et al. 2008; Kay and Gettelman 2009; Palm et al.
677 2010; Morrison et al. 2018). The difference between years 1950-1979 and years 1990-2019

678 estimates the effects of GHG-induced warming and long-term sea-ice loss on Arctic cloud changes
679 and atmospheric conditions; however, internal variability may also contribute to these differences
680 (Wettstein and Deser 2014). Further, we show new dynamic and thermodynamic processes that
681 explain why regions with sea-ice loss are more prone to enhanced cloudiness than ice-covered
682 regions. Specifically, we analyzed the seasonality and spatial patterns of changes in CAPE and
683 divergence fields that have not been examined in previous studies. We also show that local surface
684 evaporation provides an essential source of moisture for enhanced cloudiness associated with sea-
685 ice loss. To our knowledge, the long-term changes in local evaporation and meridional moisture
686 flux have not been thoroughly examined.

687 We recognize that clouds are influenced not only by conditions of the underlying surface,
688 but also the background meteorological conditions (Barton and Veron 2012; Taylor et al. 2015).
689 Our composite analyses for areas with and without large sea-ice loss minimizes the effects of other
690 factors. Further, cloud anomalies can also affect surface conditions, including sea-ice loss. Thus,
691 the SIC-cloud interactions are two-way and our correlation analysis cannot untangle the causal
692 relationship between Arctic sea-ice loss and cloud changes. For this reason, we recommend
693 analysis of climate model simulations to further assess the causal relationship between sea-ice loss
694 and clouds. Nevertheless, our results, together with previous studies (e.g., Deser et al. 2010; Screen
695 and Simmonds 2010a, b; Dai et al. 2019) have shown that sea-ice loss can increase oceanic heat
696 and water fluxes into the atmosphere during the cold season, leading to large surface warming and
697 increased upward heat and moisture transport from the surface layer into the layer above. Thus,
698 from this perspective, we interpreted the cloud differences between the areas with and without
699 significant sea-ice loss as a response to sea-ice loss.

700 Sea-ice retreat plays an essential role in enhancing Arctic surface warming (Deser et al.
701 2010; Screen and Simmonds 2010a, b) and is likely the primary cause of Arctic amplification (Dai
702 et al. 2019). Positive cloud feedbacks associated with sea-ice loss and enhanced cloudiness in
703 winter may delay cold season sea-ice formation, which has implications for future Arctic sea-ice
704 projections and surface warming. Our results may help to improve representation of Arctic clouds
705 in climate models and reduce uncertainty of future Arctic cloud feedback.

706

707 *Acknowledgements*

708 The authors acknowledge the National Science Foundation (grants AGS-2015780 and OISE-
709 1743738) for supporting this work and three anonymous reviewers that provided constructive
710 feedback to improve the manuscript. The National Center for Atmospheric Research is sponsored
711 by the National Science Foundation.

712

713 *Data Availability Statement*

714 The ERA5 data used in this study may be downloaded from
715 <https://cds.climate.copernicus.eu/#!/search?text=ERA5&type=dataset>. The CERES data is
716 available from <https://ceres.larc.nasa.gov/data/>.

717

718 REFERENCES

719

720 Abe, M., T. Nozawa, T. Ogura, and K. Takata, 2016: Effect of retreating sea ice on Arctic cloud
721 cover in simulated recent global warming. *Atmos. Chem. Phys.*, **16**, 14343-14356.
722 doi:10.5194/acp-16-14343-2.

723 Alkama, R., and Coauthors, 2020: Clouds damp the radiative impacts of polar sea ice loss. *The*
724 *Cryosphere*, **14**, 2673-2686. doi:10.5194/tc-14-2673-2020.

725 Barton, N. P., and D. E. Veron, 2012: Response of clouds and surface energy fluxes to changes in
726 sea-ice cover over the Laptev Sea (Arctic Ocean). *Clim. Res.*, **54**, 69-84.
727 doi:10.3354/cr01101.

728 Bell, B., and Coauthors, 2021: The ERA5 global reanalysis: Preliminary extension to 1950. *Q. J.*
729 *R. Meteor. Soc.*, **147**, 4186-4227. doi:10.1002/qj.4174.

730 Boeke, R. C., and P. C. Taylor, 2018: Seasonal energy exchange in sea ice retreat regions
731 contributes to differences in projected Arctic warming. *Nat. Comm.*, **9**, 5017.
732 doi:10.1038/s41467-018-07061-9.

733 Burt, M. A., D. A. Randall, and M. D. Brown, 2016: Dark warming. *J. Climate*, **29**, 705-719.
734 doi:10.1175/JCLI-D-15-0147.1.

735 Ceppi, P., F. Brient, M. D. Zelinka, and D. L. Hartmann, 2017: Cloud feedback mechanisms and
736 their representation in global climate models. *WIREs Clim. Change*, **8**, e465.
737 doi:10.1002/wcc.465.

738 Choi, Y.-S., B.-M. Kim, S.-K. Hur, S.-J. Kim, J.-H. Kim, and C.-H. Ho, 2014: Connecting early
739 summer cloud-controlled sunlight and late summer sea ice in the Arctic. *J. Geophys. Res.*
740 *Atmos.*, **119**, 11087-11099. doi:10.1002/2014JD022013.

741 Cox, C. J., T. Uttal, C. N. Long, M. D. Shupe, R. S. Stone, and S. Starkweather, 2016: The role
742 of springtime Arctic clouds in determining autumn sea ice extent. *J. Climate*, **29**, 6581-
743 6596. doi:10.1175/JCLI-D-16-0136.1.

744 Curry, J. A., W. B. Rossow, D. Randall, and J. L. Schramm, 1996: Overview of Arctic cloud and
745 radiation characteristics. *J. Climate*, **9**, 1731-1764. doi:10.1175/1520-
746 0442(1996)009<1731:OOACAR>2.0.CO;2.

747 Cuzzone, J., and S. Vavrus, 2011: The relationships between Arctic sea ice and cloud-related
748 variables in the ERA-Interim reanalysis and CCSM3. *Environ. Res. Lett.*, **6**, 014016.
749 doi:10.1088/1748-9326/6/1/014016.

750 Dai, A., D. Luo, M. Song, and J. Liu, 2019: Arctic amplification is caused by sea-ice loss under
751 increasing CO₂. *Nat. Comm.*, **10**, 121. doi:10.1038/s41467-018-07954-9.

752 Deser, C., R. Tomas, M. Alexander, and D. Lawrence, 2010: The seasonal atmospheric response
753 to projected Arctic sea ice loss in the late twenty-first century. *J. Climate*, **23**, 333-351.
754 doi:10.1175/2009JCLI3053.1.

755 Eastman, R., and S. G. Warren, 2010: Interannual variations of Arctic cloud types in relation to
756 sea ice. *J. Climate*, **23**, 4216-4232. doi:10.1175/2010JCLI3492.1.

757 England, M. R., I. Eisenmann, N. J. Lutsko, T. J. W. Wagner, 2021: The recent emergence of
758 Arctic amplification. *Geophys. Res. Lett.*, **48**, e2021GL094086.
759 doi:10.1029/2021GL094086.

760 Gettelman, A., and S. C. Sherwood, 2016: Processes responsible for cloud feedback. *Curr. Clim.*
761 *Change Rep.*, **2**, 179-189. doi:10.1007/s40641-016-0052-8.

762 Graham, R. M., and Coauthors, 2019a: Evaluation of six atmospheric reanalyses over Arctic sea
763 ice from winter to early summer. *J. Climate*, **32**, 4121-4143. doi:10.1175/JCLI-D-18-
764 0643.1.

765 Graham, R. M., S. R. Hudson, and M. Maturilli, 2019b: Improved performance of ERA5 in
766 Arctic gateway relative to four global atmospheric reanalyses. *Geophys. Res. Lett.*, **46**,
767 6138-6147. doi:10.1029/2019GL082781.

768 Hersbach, H., and Coauthors, 2020: The ERA5 global reanalysis. *Q. J. R. Meteor. Soc.*, **146**,
769 1999-2049. doi:10.1002/qj.3803.

770 Hirahara, S., M. A. Balmaseda, E. de Boisseson, and H. Hersbach, 2016: Sea surface temperature
771 and sea ice concentration for ERA5. *ERA Report Series*, **26**, ECMWF.

772 Huang, Y., and Coauthors, 2019: Thicker cloud and accelerated Arctic sea ice decline: The
773 atmosphere-sea ice interactions in spring. *Geophys. Res. Lett.*, **46**, 6980-6989.
774 doi:10.1029/2019GL082791.

775 Intrieri, J. M., M. D. Shupe, T. Uttal, and B. J. McCarty, 2002a: An annual cycle of Arctic cloud
776 characteristics observed by radar and lidar at SHEBA. *J. Geophys. Res.*, **107**, C10, 8030.
777 doi:10.1029/2000JC000423.

778 Intrieri, J. M., and Coauthors, 2002b: An annual cycle of Arctic surface cloud forcing at SHEBA.
779 *J. Geophys. Res.*, **107**, 8039. doi:10.1029/2000JC000439.

780 Jenkins, M., and A. Dai, 2021: The impact of sea-ice loss on Arctic climate feedbacks and their
781 role for Arctic amplification. *Geophys. Res. Lett.*, **48**, e2021GL094599.
782 doi:10.1029/2021GL094599.

783 Jenkins, M. T., and A. Dai, 2022: Arctic climate feedbacks in ERA5 reanalysis: Seasonal and
784 spatial variations and the impact of sea-ice loss. *Geophys. Res. Lett.*, **49**,
785 e2022GL099263. doi:10.1029/2022GL099263.

786 Kapsch, M.-L., R. G. Graverson, and M. Tjernström, 2013. Springtime atmospheric energy
787 transport and the control of Arctic summer sea-ice extent. *Nat. Clim. Change*, **3**, 744-748.
788 doi:10.1038/NCLIMATE1884.

789 Kay, J. E., and A. Gettelman, 2009: Cloud influence on and response to seasonal Arctic sea ice
790 loss. *J. Geophys. Res.*, **114**, D18204. doi:10.1029/2009JD011773.

791 Kay, J. E., T. L'Ecuyer, H. Chepfer, N. Loeb, A. Morrison, and G. Cesana, 2016: Recent
792 advances in Arctic cloud and climate research. *Curr. Clim. Change Rep.*, **2**, 159-169.
793 doi:10.1007/s40641-016-0051-9.

794 Liu, Y., S. A. Ackerman, B. C. Maddux, J. R. Key, R. A. Frey, 2010: Errors in cloud detection
795 over the Arctic using a satellite imager and implications for observing feedback
796 mechanisms. *J. Climate*, **23**, 1894-1907.

797 Liu, Y., J. R. Key, Z. Liu, X. Wang, and S. J. Vavrus, 2012: A cloudier Arctic expected with
798 diminishing sea ice. *Geophys. Res. Lett.*, **39**, L05705. doi:10.1029/2012GL051251.

799 Loeb, N. G., and Coauthors, 2018: Clouds and the Earth's radiant energy system (CERES)
800 energy balanced and filled (EBAF) top-of-atmosphere (TOA) edition-4.0 data product. *J.*
801 *Climate*, **31**, 895-918. doi:10.1175/JCLI-D-17-0208.1.

802 Monroe, E. E., P. C. Taylor, and L. Boisvert, 2021: Arctic cloud response to a perturbation in sea
803 ice concentration: The north water polynya. *J. Geophys. Res. Atmos.* **126**,
804 e2020JD034409. doi:10.1029/2020JD034409.

805 Morrison, A. L., J. E. Kay, H. Chepfer, R. Guzman, and V. Yettella, 2018: Isolating the liquid
806 cloud response to recent Arctic sea ice variability using spaceborne lidar observations. *J.*
807 *Geophys. Res. Atmos.*, **123**, 473-490. doi:10.1002/2017JD027248.

808 Morrison, A. L., J. E. Kay, W. R. Frey, H. Chepfer, and R. Guzman, 2019: Cloud response to
809 Arctic sea ice loss and implications for future feedback in the CESM1 climate model. *J.*
810 *Geophys. Res. Atmos.*, **124**, 1003-1020. doi:10.1029/2018JD029142.

811 Palm, S. P., S. T. Strey, J. Spinhirne, and T. Markus, 2010: Influence of Arctic sea ice extent on
812 polar cloud fraction and vertical structure and implication for regional climate. *J.*
813 *Geophys. Res.*, **115**, D21209. doi:10.1029/2010JD013900.

814 Philipp, D., M. Stengel, and B. Ahrens, 2020: Analyzing the Arctic feedback mechanism between
815 sea ice and low-level clouds using 34 years of satellite observations. *J. Climate*, **33**, 7479-
816 7501. doi:10.1175/JCLI-D-19-0895.1.

817 Royer, J. F., S. Planton, and M. Déqué, 1990: A sensitivity experiment for the removal of Arctic
818 sea ice with the French spectral general circulation model. *Clim. Dyn.*, **5**, 1-17.
819 doi:10.1007/BF00195850.

820 Schweiger, A., R. W. Lindsay, S. Vavrus, and J. A. Francis, 2008: Relationships between Arctic
821 sea ice and clouds during autumn. *J. Climate*, **21**, 4799-4810.
822 doi:10.1175/2008JCLI2156.1.

823 Screen, J. A., and I. Simmonds, 2010a: The central role of diminishing sea ice in recent Arctic
824 temperature amplification. *Nature*, **464**, 1334-1337. doi:10.1038/nature09051.

825 Screen, J. A., and I. Simmonds, 2010b: Increasing fall - winter energy loss from the Arctic
826 Ocean and its role in Arctic temperature amplification. *Geophys. Res. Lett.*, **37**, L16707,
827 doi:10.1029/2010GL044136.

828 Serreze, M. C., and R. G. Barry, 2011: Processes and impacts of Arctic amplification: A research
829 synthesis. *Global Planet. Change*, **77**, 85-96. doi:10.1016/j.gloplacha.2011.03.004.

830 Shupe, M. D., and J. M. Intrieri, 2004: Cloud radiative forcing of the Arctic surface: The
831 influence of cloud properties, surface albedo, and solar zenith angle. *J. Climate*, **17**, 616-
832 628. doi:10.1175/1520-0442(2004)017%3C0616:CRFOTA%3E2.0.CO;2.

833 Soden, B. J., A. J. Broccoli, and R. S. Hemmler, 2004: On the use of cloud forcing to estimate
834 cloud feedback. *J. Climate*, **17**, 3661-3665. doi:10.1175/1520-
835 0442(2004)017%3C3661:OTUOCF%3E2.0.CO;2.

836 Stroeve, J. C., T. Markus, L. Boisvert, J. Miller, and A. Barrett, 2014. Changes in Arctic melt
837 season and implications for sea ice loss. *Geophys. Res. Lett.*, **41**, 1216-1225.
838 doi:10.1002/2013GL058951.

839 Taylor, P. C., M. Cai, A. Hu, J. Meehl, W. Washington, and G. J. Zhang, 2013: A decomposition
840 of feedback contributions to polar warming amplification. *J. Climate*, **26**, 7023-7043.
841 doi:10.1175/JCLI-D-12-00696.1.

842 Taylor, P. C., S. Kato, K.-M. Xu, and M. Cai, 2015: Covariance between Arctic sea ice and
843 clouds within atmospheric state regimes at the satellite footprint level. *J. Geophys. Res.*
844 *Atmos.*, **120**, 12656-12678. doi:10.1002/2015JD023520.

845 Tiedtke, M., 1993: Representation of clouds in large-scale models. *Mon. Weather Rev.*, **121**,
846 3040-3061. doi:10.1175/1520-0493(1993)121%3C3040:ROCILS%3E2.0.CO;2.

847 Vavrus, S., 2004: The impact of cloud feedbacks on Arctic climate under greenhouse forcing. *J.*
848 *Climate*, **17**, 603-615. doi:10.1175/1520-
849 0442(2004)017%3C0603:TIOCF%3E2.0.CO;2.

850 Vavrus, S., D. Waliser, A. Schweiger, and J. Francis, 2009: Simulations of 20th and 21st century
851 Arctic cloud amount in the global climate models assessed in the IPCC AR4. *Clim. Dyn.*,
852 **33**, 1099-1115. doi:10.1007/s00382-008-0475-6.

853 Vavrus, S., M. M. Holland, and D. A. Bailey, 2011: Changes in Arctic clouds during intervals of
854 rapid sea ice loss. *Clim. Dyn.*, **36**, 1475-1489. doi:10.1007/s00382-010-0816-0.

855 Wetherald, R. T., and S. Manabe, 1988: Cloud feedback processes in a general circulation model.
856 *J. Atmos. Sci.*, **45**, 1397-1415. doi:10.1175/1520-
857 0469(1988)045%3C1397:CFPIAG%3E2.0.CO;2.

858 Wettstein, J. J. and C. Deser, 2014: Internal variability in projections of twenty-first century
859 Arctic sea ice loss: Role of the large-scale atmospheric circulation. *J. Climate*, **27**, 527-
860 550. doi:10.1175/JCLI-D-12-00839.1.

861 Wielicki, B. A., B. R. Barkstrom, E. F. Harrison, R. B. Lee III, G. L. Smith, and J. E. Cooper,
862 1996: Clouds and the Earth's radiant energy system (CERES): An Earth observing system
863 experiment. *Bull. Amer. Meteor. Soc.*, **77**, 853-868. doi:10.1175/1520-
864 0477(1996)077<0853:CATERE>2.0.CO;2.

865 Yeo, H., and Coauthors, 2022: Arctic cloud properties and associated radiative effects in the three
866 newer reanalysis datasets (ERA5, MERRA-2, JRA-55): Discrepancies and possible
867 causes. *Atmos. Res.*, **270**, 106080. doi:10.1016/j.atmosres.2022.106080.

868 Zelinka, M. D., S. A. Klein, and D. L. Hartmann, 2012: Computing and partitioning cloud
869 feedbacks using cloud property histograms. Part II: Attribution to changes in cloud
870 amount, altitude, and optical depth. *J. Climate*, **25**, 3736-3754. doi:10.1175/JCLI-D-11-
871 00249.1.

872 Zheng, Y., and Y. Ming, 2023: Low-level cloud budgets across sea-ice edges. *J. Climate*, **36**, 3-
873 18. doi:10.1175/JCLI-D-22-0301.1.

874 Zygmuntowska, M., T. Mauritsen, J. Quaas, and L. Kaleschke, 2012: Arctic clouds and surface
875 radiation – a critical comparison of satellite retrievals and the ERA-Interim reanalysis.
876 *Atmos. Chem. Phys.*, **12**, 6667-6677. doi:10.5194/acp-12-6667-2012.

877

878